Paper 30

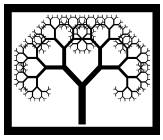

Proceedings of the Eleventh International Conference
on Computational Structures Technology,
B.H.V. Topping, (Editor),
Civil-Comp Press, Stirlingshire, Scotland

Application of Direct Strength Method Design to Distortional Buckling Resistance of Thin-Walled Steel Columns Exposed to Fire

A. Landesmann[1] and D. Camotim[2]
[1] Civil Engineering Program, COPPE
Federal University of Rio de Janeiro, Brazil
[2] Department of Civil Engineering and Architecture
ICIST, Instituto Superior Técnico, Technical University of Lisbon, Portugal

Abstract

This paper presents a numerical (shell finite element) investigation aimed at assessing the performance of the current direct strength method (DSM) provisions against distortional failure to estimate the ultimate strength of fixed-ended cold-formed steel lipped channel and rack-section columns (i) subjected to various uniform temperature distributions caused by fire conditions and (ii) exhibiting different room-temperature yield stresses, covering a wide distortional slenderness range. In particular, the work addresses how does the temperature-dependence of the steel material behaviour, which is felt through both the (reduced) Young's modulus and nominal yield stress values, influences the quality (accuracy and safety) of the column ultimate strength predictions provided by the DSM distortional strength curve. Five different temperature-dependent steel constitutive laws are considered, namely (i) two models prescribed in part 1.2 of Eurocode 3 (EC3), for cold-formed and hot-rolled steel, and (ii) three experimentally-based analytical expressions recently reported in the literature. The DSM column ultimate strength estimates are compared with the numerical failure loads obtained through geometrically and physically non-linear ANSYS shell finite element analyses incorporating critical-mode initial imperfections with small amplitudes.

Keywords: cold-formed steel columns, lipped channels, rack-sections, distortional failure, elevated temperature, constitutive models, ultimate strength, direct strength method design.

1 Introduction

The use of cold-formed steel structures has grown steadily during recent years, as they became extremely popular in different areas of the construction industry, namely (i) low rise official, residential and industrial buildings, (ii) high storage

structures and (iii) roof trussed structures. Cold-formed steel offers very flexible design solutions, exhibits a high structural efficiency (strength-to-weight ratio) and has been characterised by an enormous fabrication versatility and increasingly low production and erection costs.

The knowledge about the structural behaviour of cold-formed steel members at room temperature has advanced considerably in the last few years and, moreover, such advances have been incorporated in design specifications at a fairly rapid pace. Since it is well known that many cold-formed steel members are prone to distortional failure, the current design specifications include provisions dealing with this collapse mode. In particular, the direct strength method (DSM – *e.g.* [1]), which has already been incorporated in the current versions of the North-American [2], Australian/New Zealand [3] and Brazilian [4] specifications for cold-formed steel structures, includes specific provisions (strength curves) for the design of columns and beams against distortional failure – their application requires only the knowledge of the distortional buckling and yield loads or moments. However, such provisions/curves were developed and validated for cold-formed steel members at room temperature and it is still unknown whether they can also be adopted (with or without modifications) to estimate the ultimate strength of members under elevated temperatures caused by fire conditions, which alter considerably the steel constitutive law, namely its Young's modulus, yield strength and non-linearity.

Indeed, the high "section factor"[1], associated with the use of (i) high-strength steels and (ii) very slender cross-sections, is responsible for making cold-formed steel construction particularly vulnerable to fire conditions. Thus, the current design methods require the use of expensive fireproof materials, aimed at protecting the steel structures from an excessive heat increase due to fire hazards. This requirement quite often leads to overly conservative and unduly uneconomical structural designs. Moreover, it is fair to say that the research activity devoted to cold-formed steel members under fire conditions only started in this century and is still rather scarce, as attested by the relatively small number of available publications on the subject. Without claiming to be complete, such publications report essentially the work done by Outinen *et al.* [5], Kaitila [6], Feng *et al.* [7-11], Lee *et al.* [12], Feng and Wang [13, 14], Chen and Young [15-18], Ranawaka [19], Ranawaka and Mahendran [20-22], Landesmann and Camotim [23-26], and Shahbazian and Wang [27-29]. Moreover, only a small fraction of the above studies addresses failures stemming from the occurrence of distortional buckling, an instability phenomenon that often governs the behaviour and strength of lipped members with intermediate unrestrained lengths.

1.1 Motivation, objective and scope of this work

Several researchers, namely Outinen and Makelainen [30], Lee *et al.* [12], Mecozzi and Zhao [31], Zhao *et al.* [32], Chen and Young [16], Ranawaka and Mahendran

[1] The heating rate of a steel cross-section depends on its dimensions, namely the so-called "section factor", given by Hp/A, where Hp and A are the cross-section (i) perimeter exposed to the fire and (ii) area. Large Hp/A values imply a high susceptibility to fire effects, *i.e.*, a high need for the use of fireproof materials.

[20], Kankanamge and Mahendran [33] and Wei and Jihong [34], investigated experimentally the variation of the cold-formed steel constitutive law with the temperature, and proposed experimentally-based analytical expressions to model the cold-formed steel material behaviour at elevated temperatures. The temperature-dependence is taken into account through reduction factors applied to the steel Young's modulus, proportional limit stress, yield stress and ultimate stress. However, there are significant discrepancies between the reductions factors proposed in the various works, which also differ from those prescribed, for fire conditions, in the current steel design codes. Furthermore, in the course of numerical investigations on the distortional on the post-buckling behaviour and ultimate strength of lipped channel and rack-section columns under fire conditions, the authors [23-26] found that, at least for the particular column geometries analysed and temperature-dependent material models considered, the quality (accuracy and safety) of the ultimate load estimates determined with the current DSM distortional design/strength curve/expressions (at elevated temperatures) exhibited a mild dependence on the temperature [26]. This finding provided the motivation for the present work, which considers two additional models to simulate the cold-formed steel material behaviour at elevated temperatures and aims at contributing towards answering the following question: "how does the temperature dependence of the steel material behaviour influence the quality/safety of the column ultimate load estimates provided by the current DSM distortional strength design curve?".

1.2 Outline of the paper

The paper begins by presenting a literature survey concerning the available cold-formed steel constitutive laws at elevated temperatures caused by fire conditions, devoting particular attention to the different reductions factors proposed to model the erosion of the steel Young's modulus and yield stress. The main output of this literature review is the selection of *five* representative temperature-dependent constitutive laws to model the cold-formed steel material behaviour, which are subsequently adopted to (i) perform the distortional failure shell finite element analyses (SFEA) and (ii) determine the DSM predictions corresponding to the numerical failure loads. The next step consists of performing sequences of "trial and error" buckling analyses, in order to select *two* fixed-ended column geometries (cross-section dimensions and lengths), one involving a lipped channel and the other a rack-section, that ensure distortional buckling and failure modes as "pure" as possible – *i.e.*, the selected columns exhibit distortional critical buckling loads that are significantly lower than their local and global counterparts. Then, after briefly addressing the shell finite element model employed to perform the geometrically and materially non-linear analyses in the code ANSYS [35], (i) illustrative numerical results concerning the column distortional post-buckling behaviour and ultimate strength are presented and discussed, and (ii) a *parametric stud*y is carried out, in order to assemble a fairly extensive fixed-ended lipped and rack-section column numerical ultimate strength "data bank". The columns analysed (i) display the five temperature-dependent cold-formed steel constitutive laws selected earlier, (ii) exhibit several room temperature yield stresses, covering a wide distortional

slenderness range, (iii) contain critical-mode (distortional) initial geometrical imperfections with small amplitude (equal to *10%* of the wall thickness *t*), and (iv) are compressed under various uniform temperatures that may be as high as *600* ºC. Finally, after comparing the trends of the numerical column ultimate loads with those exhibited by some experimental values reported in the literature, the available (numerical and experimental) failure loads under various temperatures are used to assess the quality (accuracy and safety) of the estimates provided by the current DSM distortional strength curve. In particular, the comparison between the column ultimate loads and their DSM predictions makes it possible (i) to appraise how the current distortional strength curve is able to cope with the constitutive law variation with the temperature, for the different models, and also (ii) to suggest a few preliminary modifications/adjustments to account for the temperature effects.

2 Steel Constitutive Laws at Elevated Temperatures

The search for accurate methodologies to ensure the fire safety design of cold-formed steel members must begin with a fairly accurate knowledge on the temperature-dependence of the cold-formed steel thermal and mechanical properties, which is often very substantial. In addition, it is now widely recognised that the reduction factors applicable to hot-rolled steel grades do not apply to the cold-formed ones. Indeed, as stated by Sidey and Teague [36] a while ago, the strength reduction in cold-formed steels at elevated temperatures may be *10-20%* higher than that occurring in hot-rolled steels – this is due to different metallurgical composition and molecular surface effects. Furthermore, Kankanamge and Mahendran [33] recently found that cold-formed steels under elevated temperatures are likely to lose the additional strength acquired during the cold-working process at ambient temperature.

Although design standards, such as BS5950-8 [37] or EC3-1.2 [38], contain provisions specifying the mechanical properties of cold-formed steels at elevated temperatures, they do not include accurate reduction factors for the Young's modulus and yield stress. Indeed, BS5950-8 (i) provides no Young's modulus reduction factor (the key feature to assess the column buckling behaviour), (ii) only includes yield stress reduction factors for temperatures below *600* ºC, and (iii) considers proof stresses corresponding to *0.5*%, *1.5*% and *2.0*% strain levels, in contrast with the current common practice of dealing with *0.2*% proof stresses. On the other hand, EC3-1.2 treats cold-formed steel members similarly to thin-walled (*i.e.*, *Class 4*) hot-rolled and welded ones. The only differences, with respect to the remaining (Class 1, 2, 3) hot-rolled and welded members, involve the (i) effective yield stress definition, corresponding to *0.2%* residual strain (after unloading), instead of the *2%* absolute strain, and (ii) reduction factor, given in Table E.1 of Annex E, instead of Table 3.1 of 3.2.1[2].

[2] EC3-1.2 also recommends considering the load-bearing capacity of Class 4 members exhausted at the "critical temperature" *350*ºC. The findings reported in this work clearly show that this limit is too conservative.

In order to overcome the lack of reliable information on the temperature-dependence of the mechanical properties of cold-formed steel members, essential for their design in fire conditions, Lee *et al.* [12], Mecozzi and Zhao [31], Chen and Young [16], Ranawaka and Mahendran [20], Kankanamge and Mahendran [33] and Wei and Jihong [34] undertook experimental investigations, based on the performance of tensile coupon tests at elevated temperatures, and came up with several proposals of experimentally-based analytical expressions providing stress-strain curves to be used in the fire safety design of cold-formed steel members. The analysis of the test data showed that the cold-formed steel yield stress reduction factor is highly dependent on the strain level assumed to correspond to the measured yield stress – a conservative approach consists of adopting the reduced *0.2*% proof stress as the design strength, as has been done in EC3-1.2 [38]. In the above proposals, the temperature-dependence is always accounted for by means of reduction factors applicable to the steel Young's modulus (k_e), nominal yield stress (k_y) and proportional limit stress (k_p). Figs. 1(a)-(b) make it possible to compare the k_e and k_y temperature-dependences prescribed by EC3-1.2, for hot-rolled (HR) and cold-formed (CF) steels, with those proposed by Chen and Young [16] (CY), Ranawaka and Mahendran [20] (RM) and Wei and Jihong [34] (WJ) – these five models were adopted to carry out the research work reported in this paper and will be presented in some detail further ahead. One readily observes that there are visible differences between the curves concerning the various constitutive laws – in particular, note that the two EC3-1.2 HR steel reduction factors are higher than their four counterparts for most of the considered temperature range, which is bound to have a relevant impact on the column buckling, post-buckling and ultimate strength behaviours analysed in this work. Fig. 1(c) shows the qualitative differences between the steel stress-strain curves ($\sigma_T/\sigma_{y.20}$ *vs.* ε, where σ_T is the applied stress at a given temperature, normalised with respect to the room temperature yield stress $\sigma_{y.20}$) prescribed by the five models for *T=20* ºC, *T=400* ºC and *T=600* ºC. Note that, regardless of the material model considered, the non-linearity of the stress-strain curve increases substantially with the temperature (for *T=20* ºC, the EC3-1.2 model prescribes a bi-linear constitutive law, defining an elastic-perfectly plastic material).

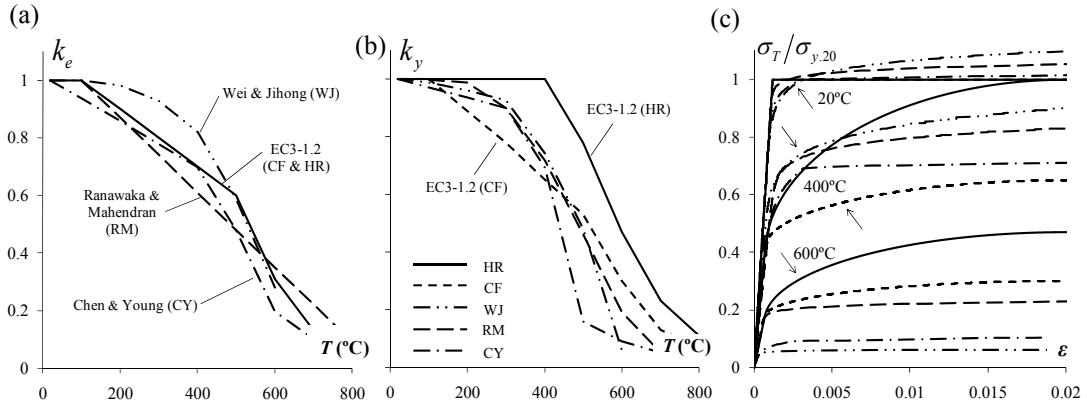

Figure 1: Variation of (a) k_e and (b) k_y with the temperature ($T \leq 800$ °C), and (c) steel stress-strain curves prescribed by the HR, CF, CY, RM, WJ models (*T=20-400-600* ºC – $\varepsilon \leq 2\%$).

2.1 Eurocode 3 Part-1.2 models

EC3-1.2 [38] provides analytical expressions to define the steel constitutive law at elevated temperatures that are based work by Kirby and Preston [39] on hot-rolled steel grades and, thus, may not model accurately the temperature-dependence of the cold-formed steel stress-strain curve. The effect of creep is implicitly considered and the material models are valid for heating rates between *2* and *50 K/min*. The corresponding stress-strain curve, given by

$$\sigma_T = \begin{cases} \varepsilon \cdot E_T & \text{for } \varepsilon \le \varepsilon_{p.T} \\ \sigma_{p.T} - c + (b/a)\left[a^2 - \left(\varepsilon_{y.T} - \varepsilon\right)^2\right]^{0.5} & \text{for } \varepsilon_{p.T} < \varepsilon < \varepsilon_{y.T} \\ \sigma_{y.T} & \text{for } \varepsilon_{y.T} \le \varepsilon \le \varepsilon_{u.T} \end{cases}, \quad (1)$$

$$a^2 = \left(\varepsilon_{y.T} - \varepsilon_{p.T}\right)\left(\varepsilon_{y.T} - \varepsilon_{p.T} + c/E_T\right),\ b^2 = c\left(\varepsilon_{y.T} - \varepsilon_{p.T}\right)E_T + c^2,$$

$$c = \frac{\left(\sigma_{y.T} - \sigma_{p.T}\right)^2}{\left(\varepsilon_{y.T} - \varepsilon_{p.T}\right)E_T - 2\left(\sigma_{y.T} - \sigma_{p.T}\right)}$$

is divided into three different regions, associated with distinct strain ranges. Note that (i) the effective yield stress $\sigma_{y.T}$ is defined differently by $\varepsilon_{y.T}$ for hot-rolled and cold-formed steels (*2%* absolute vs. *0.2%* residual strains) and that (ii) the stress-strain curve shape is strongly influenced by the temperature, namely via the proportionality limit strain ($\varepsilon_{p.T}=\sigma_{p.T}/E_T$)[3]. The initial part of the well-defined yield plateau exhibited by the $T=20$ °C curve is replaced by a strain-hardening region that becomes more pronounced as the temperature increases. The stress-strain curve (i) is linear elastic, with slope E_T, up to the proportional limit $\sigma_{p.T}$, then (ii) becomes elliptic in the transition between the elastic and plastic ranges, up to $\sigma_{y.T}$ (effective yield stress), and (iii) ends with a yield plateau up to the limit strain $\varepsilon_{u.T}=0.15$.[4]

2.2 Chen and Young model

The experimentally-based constitutive model proposed by Chen and Young [16] exhibits a Ramberg-Osgood [40] format, which was previously adopted by Mirambell and Real [41] and Rasmussen [42] to describe stainless steel constitutive laws at room temperature. This means that the corresponding temperature-dependent equations, given by

[3] The EC3-1.2 model extends the stress-strain curve further, including strain-hardening effects for $T<400$ °C (these effects are negligible for temperatures above *400*ºC) – such extension is not considered in this work.

[4] Recall that the E, $\sigma_{p.T}$, $\sigma_{y.T}$ and E_T values depend on the temperature T through the coefficients (i) k_e and k_p, given in Table 3.1 (HR and CF), and (ii) k_p, given either in Table 3.1 (HR) or in Table E.1 (CF).

$$\varepsilon_T = \begin{cases} \dfrac{\sigma_T}{E_T} + 0.002\left(\dfrac{\sigma_T}{\sigma_{y.T}}\right)^{n_T} & \text{for } \sigma_T \le \sigma_{y.T} \\ \dfrac{\sigma_T - \sigma_{y.T}}{E_{y.T}} + \varepsilon_{u.T}\left(\dfrac{\sigma_T - \sigma_{y.T}}{\sigma_{u.T} - \sigma_{y.T}}\right)^{m_T} + \varepsilon_{y.T} & \text{for } \sigma_T > \sigma_{y.T} \end{cases} , \quad (2)$$

express the strain in terms of the stress by means of a two-part curve with a continuous derivative at the transition point, occurring for $\sigma_T = \sigma_{y.T}$ (σ_T is the applied stress at temperature T), where E_T and $\sigma_{y.T}$ are the initial Young's modulus and effective yield stress, associated with the "elastic" limit strain $\varepsilon_{y.T}$. The constitutive law temperature-dependence is felt through various quantities, obtained from the expressions

$$E_{y.T} = \frac{E_T}{1 + 0.002 \cdot n_T \left(E_T / \sigma_{y.T}\right)}, \; n_T = 20 - 0.6\sqrt{T}, \; m_T = 1 + T/350, \; \frac{\varepsilon_{u.T}}{\varepsilon_{u.20}} = 0.2 - \frac{(T-1000)^6}{-1.1 \cdot 10^{18}}$$

$$\frac{\sigma_{u.T}}{\sigma_{u.20}} = \begin{cases} 1 - \dfrac{(T-22)^6}{1.5 \cdot 10^4} & \text{for } 20 \le T \le 320\ ^\circ C \\ 0.026 - \dfrac{(T-1000)^4}{-2.24 \cdot 10^{11}} & \text{for } 320 < T \le 1000\ ^\circ C \end{cases},$$

where (i) $E_{y.T}$ is the inverse of the strain-stress slope at the transition point and (ii) the constants appearing in the various expressions were calibrated through tensile coupon test results. The test program included steel grades *G550* and *G450*, with nominal yield stresses of *550 MPa* and *450 MPa*, and the coupon plate thicknesses were *1.0 mm* and *1.9 mm*. Both steady state and transient tests were conducted at various temperatures, up to *1000*ºC.

2.3 Ranawaka and Mahendran model

Ranawaka and Mahendran [20] performed an extensive experimental program comprising the testing of tensile coupons (i) with three nominal thicknesses (*0.60-0.80-0.95 mm*), (ii) made of *G550* and *G250* steel grades, with nominal yield stresses *550 MPa* and *250 MPa*, and (iii) subjected to eight uniform temperatures (*20-100-200-350-500-600-650-800* ºC). The output of this experimental program was also a Ramberg-Osgood type constitutive model, according to which ε_T is given by the expression

$$\varepsilon_T = \frac{\sigma_T}{E_T} + \beta\left(\frac{\sigma_{y.T}}{E_T}\right)\left(\frac{\sigma_T}{E_T}\right)^{\eta_T} , \quad (3)$$

where β=*0.86* (value also adopted by Outinen [43]) and the temperature-dependence of η_T is given, for the *G550* steel (sole model adopted in this work – applied to all steel grades), by

$$\eta_T = -3.05 \cdot 10^{-7} T^3 + 0.0005 \cdot T^2 - 0.2615 \cdot T + 62.653 \quad \text{for } 20 \le T \le 800\ ^\circ C \quad . \quad (4)$$

Out of the various analytical expressions that were developed to quantify the constitutive law temperature-dependence, those considered in this work concern the variation of the Young's modulus and yield stress with the temperature *T*, which read

$$\frac{E_T}{E} = \begin{cases} 1 & \text{for } 20 \le T \le 100\ ^\circ C \\ -0.0013T + 1.1297 & \text{for } 100 < T \le 800\ ^\circ C \end{cases} \quad (5)$$

$$\frac{\sigma_{y.T}}{\sigma_{y.20}} = 1.848 \cdot 10^{-11} T^{3.98} - 1.91 \cdot 10^{-8} T^3 + 3.625 \cdot 10^{-6} T^{1.997} + 0.99 \quad \text{for } 20 \le T \le 800\ ^\circ C \,. \quad (6)$$

2.4 Wei and Jihong Model

Wei and Jihong [34] performed a series of steady state and transient tests on *1 mm* thick tensile coupons made of *G550* steel (nominal yield stress *550 MPa*). As the previous authors [16, 20], they proposed an experimentally-based Ramberg-Osgood type stress-strain curve,

$$\varepsilon_T = \frac{\sigma_T}{E_T} + 0.002 \left(\frac{\sigma_T}{\sigma_{y.T}} \right)^{n_T} \quad , \quad (7)$$

which is valid for $\sigma_T \le \sigma_{u.T}$ and where the temperature-dependence is felt through (i) the parameter η_T, given by

$$\eta_T = aT^2 + bT + c \quad , \quad (8)$$

where the coefficients *a*-*c* vary with the temperature interval and test type (steady state or transient), and (ii) the reduction factors applicable to the Young's modulus E_T (k_e), yield stress $\sigma_{y.T}$ (k_y) and ultimate strength $\sigma_{u.T}$ (k_u), for *G550* steel, which are obtained from

$$k = a\left(T - b\right)^c + d \quad , \quad (9)$$

an expression applicable to all reduction factors and where the three coefficient sets *a*-*d* vary again with the temperature interval and test type. Even if transient test results are said to be more accurate (steady state ones lead to fire resistance overestimations in cold-formed steel structures), such results were obtained only for

temperatures below *550* ºC. Thus, in order to cover temperatures up to *600* ºC, only steady state stress-strain curves are used here.

3 Column Geometry Selection – Buckling Behaviour

The cold-formed steel fixed-ended (end sections locally and globally fixed with warping prevented) lipped channel and rack-section columns analysed in this work exhibit the cross-section dimensions and elastic constants given in Table 1. These cross-section dimensions make it possible to select column lengths ensuring pure distortional critical buckling modes. The buckling analyses required to identify the above column geometries were carried out in the code GBTUL [44, 45], based on Generalized Beam Theory (GBT). The curves depicted in Figure 2 provide the variation of the elastic critical buckling stress σ_{cr}, normalised with respect to the room temperature critical distortional buckling stress $\sigma_{cr.D.20}$, with the column length L (logarithmic scale) and temperature T, for the lipped channel and rack-section columns. Three temperatures are considered (room temperature *20* ºC, *400* ºC and *600* ºC) and the HR EC3-1.2 constitutive model is adopted. Also shown are the critical (distortional) buckling mode shapes of the two column sets analysed, which correspond to L_D=*132 cm* (lipped channel) and L_D=*242 cm* (rack-section). Note that (i) any given buckling curve can be obtained through a "vertical translation" of the top one, with a magnitude that depends exclusively on the Young's modulus erosion due to the rising temperature (Poisson's ratio υ is deemed temperature-independent and equal to *0.3*)[5], and that (ii) the critical distortional stress ($\sigma_{cr.D.T}$) corresponds to the same length (L_D) for each column cross-section.

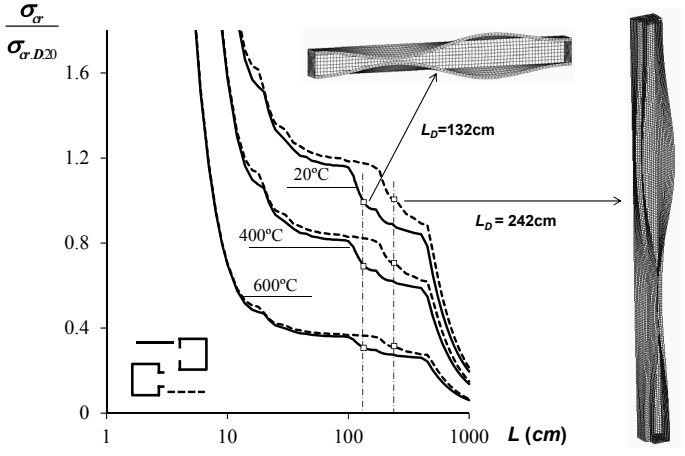

Figure 2: Variation of the buckling curves $\sigma_{cr}/\sigma_{cr.D.20}$ *vs.* L with T (HR EC3-1.2 model).

[5] Naturally, the Young's modulus reduction factor k_e, whose temperature-dependence is illustrated in Figure 1(a), makes it possible to quantify the decrease in column critical buckling load $P_{cr.T}$ for a given length.

Column	b_1 (mm)	b_2 (mm)	b_3 (mm)	b_4 (mm)	t (mm)	E (GPa)	L_D (cm)	$\sigma_{cr.D.20}$ (MPa)
Rack	134.7	80.8	24.2	47.1	2.3	210	242	253.7
Lipped C	130	100	12.5	–	2.0	205	132	191.5

Table 1: Column cross-section dimensions, elastic constants, lengths and critical stresses.

4 Column Post-Buckling Behaviour and Ultimate Strength

After briefly addressing the numerical (SFE) model used to perform the geometrically and materially non-linear analyses, results concerning the influence of the steel constitutive law on the column distortional post-buckling behaviour and strength are presented and discussed.

4.1 Numerical model

The column distortional post-buckling analyses were carried out in the code ANSYS [35], employing a shell finite element model previously validated by the authors [23-25] that involves column discretisations into fine SHELL181 (ANSYS nomenclature) element meshes – 4-node shear deformable thin-shell elements with six degrees of freedom per node and full integration. Both the residual stresses and corner effects were neglected. The analyses (i) were performed by means of an incremental-iterative technique combining Newton-Raphson's method with an arc-length control strategy and (ii) simulate the response of columns subjected to an uniform temperature distribution (*i.e.*, they are deemed engulfed in flames and, thus, share the surrounding air temperature [46]) and subsequently axially compressed up to failure – steady state analyses providing failure loads[6].

The columns analysed contained initial geometrical imperfections with a critical-mode (distortional) shape and amplitude equal to *10%* of the wall thickness *t*. Due to the column distortional post-buckling asymmetry, these initial imperfections involve outward (lipped channel columns) and inward (rack-section columns) flange-lip motions – those leading to lower post-buckling strengths [47, 48][7]. Each critical buckling mode shape was determined by means of an ANSYS buckling analysis,

[6] Note that the authors [23, 24] have shown that the failure loads yielded by the steady state analyses match the more realistic failure temperatures obtained through the "corresponding" transient analyses (axially compressed columns heated up to failure), which means that the column (distortional) failure under fire conditions can be fully investigated by resorting only to failure loads.

[7] Obviously, the distinction between distortional initial geometrical imperfections involving inward and outward flange-lip motions only matters in columns buckling in modes exhibiting odd half-wave numbers.

performed with exactly the same shell finite element mesh employed to carry out the subsequent non-linear (post-buckling) analysis – this procedure makes it very easy to "transform" the buckling analysis output into a non-linear analysis input. The column end sections were fixed, a support condition modelled by means of rigid end-plates attached to the end cross-section centroids and only allowed to exhibit axial translations. Finally, the axial compression was applied by means of two point loads acting on the end-plate points corresponding to the cross-section centroids. Such forces are applied in small increments, by means of the ANSYS automatic load stepping procedure.

The multi-linear stress-strain curve available in ANSYS code is adopted to model the steel material behaviour. Its first branch models the linear elastic range, up to the proportional limit stress and with a slope equal to Young's modulus. The following branches stand for the inelastic range, which accounts for (kinematic) strain-hardening. Finally, note that, since the distortional post-buckling analyses carried out involve large inelastic strains, the nominal (engineering) static stress-strain curve is replaced by a relation between the true stress and the logarithmic plastic strain. The variation of the cold-formed steel material behaviour with the temperature is described by the five constitutive models described earlier in 2.1-2.4.

4.2 Elastic-plastic post-buckling behaviour and ultimate strength

Attention now is devoted to the qualitative and quantitative influence of the temperature-dependent steel constitutive law on the column elastic-plastic distortional post-buckling and ultimate strength behaviours. Figure 3 shows a sample of the geometrically and materially non-linear equilibrium paths $P/P_{cr.20}$ *vs.* $|\delta|/t$, determined to obtain the ultimate loads $P_{u.T}$ (identified by white circles)[8]. As for Figure 4, it shows the von Mises stress distributions occurring at the distortional collapse ($P=P_{u.D.T}$). Both figures concern analyses of lipped channel and rack-section columns made of $\sigma_{y.20}=550\ MPa$ steel (room temperature yield stress) and subjected to temperatures $T=100\text{-}400\text{-}600$ ºC – the steel constitutive law temperature-dependence is simulated by the HR EC3-1.2 model. These elastic-plastic distortional post-buckling and ultimate strength results prompt the following remarks:

(i) Obviously, the ultimate strength decreases as the temperature T rises for all columns.

(ii) Regardless of the temperature and constitutive model, the $P_u/P_{cr.20}$ values of the lipped channel columns are consistently higher than their rack-section column counterparts.

(iii) As expected, regardless of the cross-section shape and temperature, the $P_u/P_{cr.20}$ curves concerning the HR EC3-1.2 model are practically always above those stemming from the remaining four constitutive models. This is just a direct consequence from the lower Young's modulus and yield stress reduction

[8] These equilibrium paths relate the applied load, normalised with respect to the corresponding column critical buckling load $P_{cr.D}$, to the normalised displacement ratio $|\delta|/t$, where $|\delta|$ is the absolute value of the maximum vertical displacement occurring along the flange-stiffener longitudinal edges and t is the wall thickness.

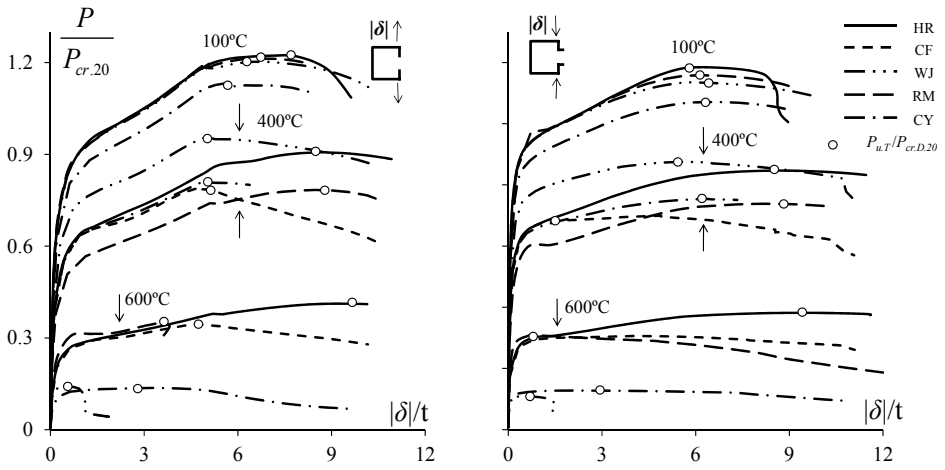

Figure 3: Lipped channel and rack-section column distortional post-buckling equilibrium paths for $\sigma_{y.20}$=550 *MPa*, *T=100-400-600* ºC and constitutive models HR, CF, CY, RM, WJ.

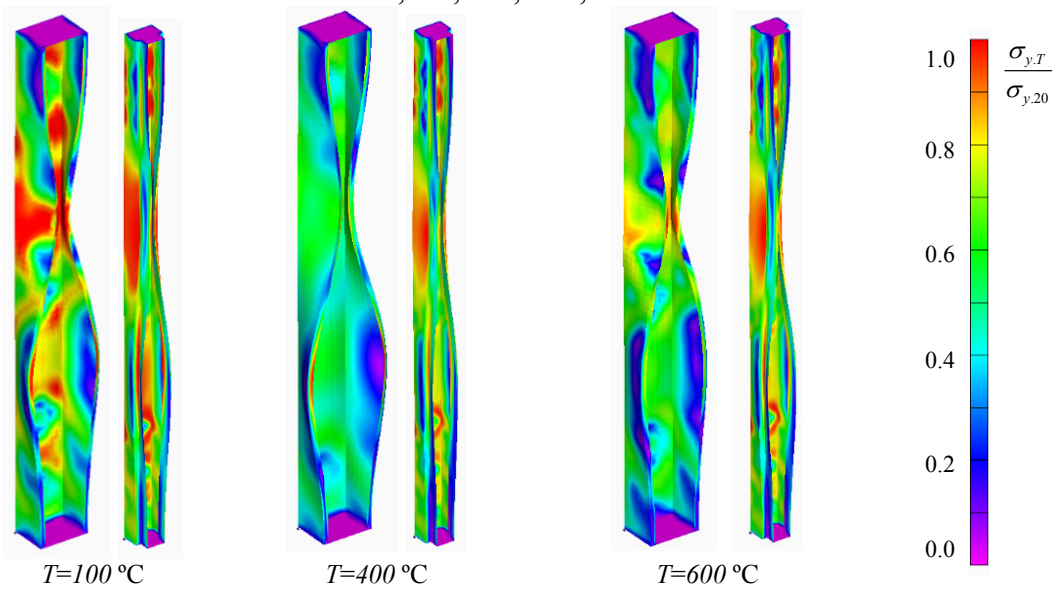

Figure 4: Lipped channel and rack-section column von Mises stress distributions at collapse (distortional) for $\sigma_{y.20}$=550 *MPa*, *T=100-400-600* ºC and the HR constitutive model.

factors, as illustrated in Figures 1(a)-(b).

(iv) For the columns subjected to *T=100* ºC, the $P_u/P_{cr.D}$ values are ordered according to the constitutive model sequence HR/CF–RM–WJ–CY, *i.e.*, following the values of the reduction factors k_e and k_y (note that, for *T=100* ºC, both factors are ordered in the same sequence). Although this picture is slightly altered for the higher temperatures, the $P_u/P_{cr.D}$ values also follow the reduction factor trend, which confirms its relevance on the column post-buckling behaviour and ultimate strength. For columns subjected to *T=400* ºC and *T=600* ºC, the $P_u/P_{cr.D}$ values are ordered according to the sequences

WJ–HR–CY–RM–CF and HR–RM–CF–CY–WJ, respectively. One readily notices the shift of the WJ constitutive model, which is due to the fact that, for these particular temperatures, it prescribe clearly the highest k_e ($T=400$ ºC) and the lowest k_y ($T=600$ ºC). The above $P_u/P_{cr.D}$ sequences apply to both cross-section shapes.

(v) Since the thermal action effects are negligible (uniform temperature and "free-to-deform" columns), the distortional failure modes are virtually identical in the three column pairs, *i.e.*, they do not depend on the temperature. Moreover, the von Mises stress distributions are also qualitatively rather similar – the highest stresses always occur in the vicinity of the lip free ends. It is also worth noting that the collapse is always triggered by the yielding of the web-flange edge regions in the vicinity of the half-wave central regions. Quantitatively speaking, the stress values obviously decrease as the temperature rises and continuously erodes the steel material behaviour.

(vi) Finally, it should be mentioned that no clear trend has been detected concerning the influence of the temperature on the amount of column elastic-plastic strength reserve and ductility prior to failure.

5 Parametric Study

This section presents and discusses the results of the parametric study carried out to gather ultimate strength data that will enable the assessment of the DSM estimates. This parametric study involved a total of *420* columns, corresponding to all possible combinations of the (i) *2* fixed cold-formed column geometries defined in Table 1 (lipped channel and rack-section), (ii) *5* constitutive models described in section 2 (HR, CF, CY, RM, WJ), (iii) *7* uniform temperatures (*T=20-100-200-300-400-500-600* ºC*)* and, (iv) *6* steel grades, with room temperature yield stresses $\sigma_{y.20}$*=250-355-550-700-1000-1200 MPa* – values selected to cover wide distortional slenderness ranges for all column sets: $\overline{\lambda}_{D.T}$ varies from *0.99* to *3.56* (HR), *0.98* to *2.80* (CF), *0.57* to *2.69* (CY), *0.74* to *2.76* (RM) and *0.45* to *2.50* (WJ).

5.1 Numerical ultimate strengths

Tables A1 to A7, presented in annex, contain (i) all the numerical column ultimate loads ($P_{u.T}$) obtained, normalised with respect to the corresponding squash loads ($P_{y.T}=A\cdot f_{y.T}$), and (ii) the associated distortional slenderness values ($\overline{\lambda}_{D.T}$). Those seven ultimate load sets (one per temperature) are also plotted in Figures 5(a) (room temperature $T=20$ ºC) and 6 (elevated temperatures $T=100-200-300-400-500-600$ ºC), together with several available experimental results reported by Schafer [1] ($T=20$ ºC) and Ranawaka [19] (elevated temperatures[9]). The observation of these seven plots makes it possible to conclude that:

[9] The results concern the following column dimensions and yield stresses: (i) $b_1=30$, $b_2=30$, $b_3=5$, $t=0.60\,mm$, $\sigma_{y.20}=315-675\,MPa$ and $L=20\,cm$ (lipped channels) and (ii) $b_1=40$, $b_2=30$, $b_3=5$, $b_4=10$, $t=0.60-0.80-0.95\,mm$, $\sigma_{y.20}=250-550\,MPa$ and $L=22-24-28\,cm$ (rack-section columns).

(i) As it would be logical to anticipate, the six $P_{u.T}/P_{y.T}$ *vs.* $\overline{\lambda}_{D.T}$ "clouds" follow trends that can be accurately described by Winter-type strength/design curves. Moreover, the "vertical dispersion" is acceptable in all of them, even if the stocky columns subjected to $T=600$ ºC and analysed with the CY model exhibit considerably lower ultimate loads, due to higher reduction factors – recall that this model stipulates a sudden drop of the yield stress reduction factor for

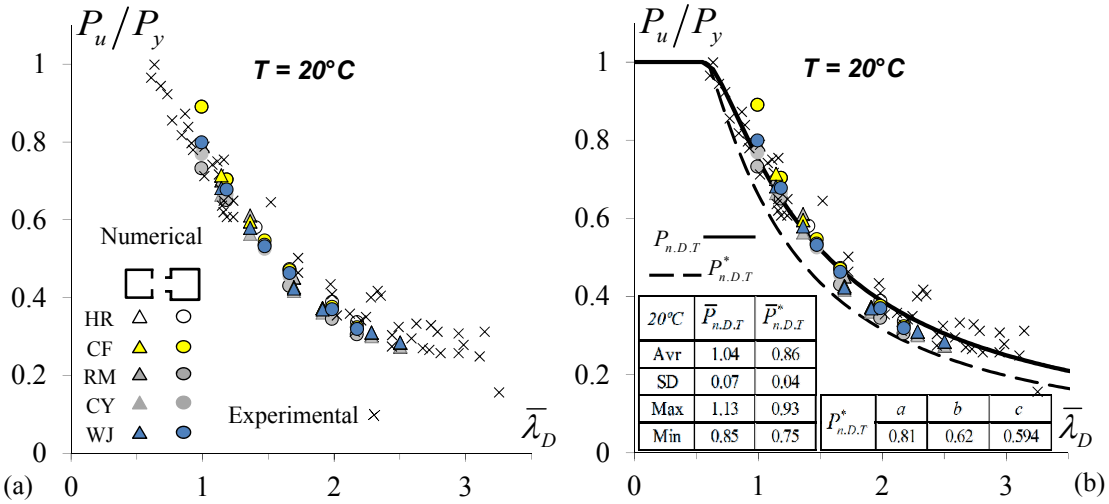

Figure 5: (a) Numerical and experimental room temperature P_u/P_y values plotted against $\overline{\lambda}_D$, and (b) their comparison with the current and modified DSM distortional strength curves.

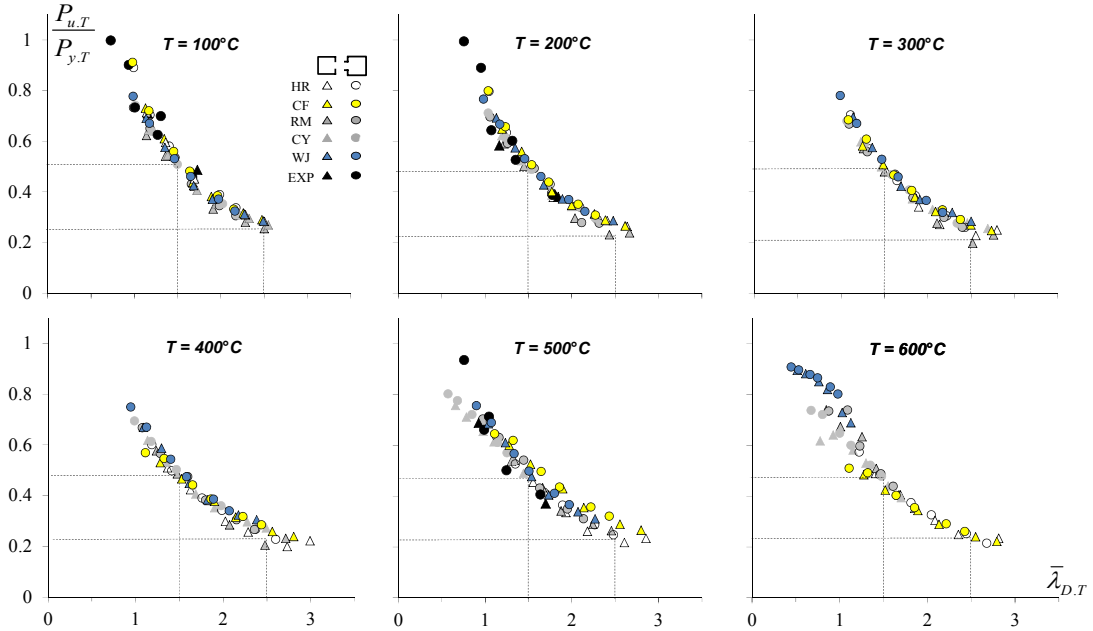

Figure 6: Numerical and experimental $P_{u.T}/P_{y.T}$ values plotted against $\overline{\lambda}_{D.T}$ ($T>20$ ºC).

$T \geq 500$ ºC[10]. In the columns subjected to $T=600$ ºC and analysed with the WJ model, the reduction factor combination ($k_e=0.281$ and $k_y=0.057$) leads to only quite stocky columns (the stockiest of all the columns analysed): $\overline{\lambda}_{D.T}$ ranges from *0.45* to *0.98* (rack-section) and from *0.51* to *1.13* (lipped channels). The corresponding $P_{u.T}/P_{y.T}$ values are fairly well aligned (very small vertical dispersion) along a curve that seems to "point" at about $0.92 P_{y.T}$ for $\overline{\lambda}_{D.T} \approx 0$.

(ii) The $P_{u.T}/P_{y.T}$ values of the $T=20$ ºC (and $T=100$ ºC) columns are above those concerning the columns acted by higher temperatures ($T>100$ ºC). The dashed grid lines included in Figure 6, associated with $\overline{\lambda}_{D.T}=1.5$ and $\overline{\lambda}_{D.T}=2.5$, provide a good visualisation of this assertion – the $T=100$ ºC column horizontal lines lie a bit above the remaining ones, which are located roughly at the same level.

(iii) The experimental results plotted in Figure 5(a) ($T=20$ ºC) and 6 ($T=100$-200-500 ºC) "mingle" well with the numerical values and follow exactly the same Winter-type trend.

6 Direct Strength Method (DSM) Design Considerations

This section deals with the adequacy of the current direct strength method (DSM) distortional strength curve to predict the ultimate strength of the cold-formed steel lipped channel and rack-section columns analysed in this work, which (i) exhibit five different temperature-dependent steel constitutive laws and (ii) exhibit distortional failure modes at all the temperatures considered – in particular, it is intended to assess whether the quality of the DSM ultimate load estimates is affected by the temperature-dependence. It is worth recalling that the DSM (i) stems from on original idea of Hancock *et al.* [49], (i) was first formally proposed by Schafer and Peköz [50], (iii) has been subsequently improved, mostly due to Schafer's efforts [1] and (iv) has already been included in the current versions of the North American [2], Australian/New Zealand [3] and Brazilian [4] specifications for cold-formed steel structures, but always for room temperature only. In this context, the nominal ultimate load of cold-formed steel columns failing in distortional modes is given by the expressions

$$P_{n.D} = \begin{cases} P_y & \text{for } \overline{\lambda}_D \leq 0.561 \\ P_y \left[1 - 0.25 \left(P_{cr.D}/P_y \right)^{0.6} \right] \left(P_{cr.D}/P_y \right)^{0.6} & \text{for } \overline{\lambda}_D > 0.561 \end{cases} , \quad (10)$$

where (i) $P_{cr.D}$ and P_y are the column (distortional) critical buckling squash loads and (ii) the column distortional slenderness, given $\overline{\lambda}_D = (P_y/P_{cr.D})^{0.5}$.

[10] Both the RM and CY constitutive models are based on high-strength steel (*G550*) parameters. However, note that the yield stress erosion differs considerably in low and high-strength steels in the *200-500*ºC range – *e.g.*, for $T>400$ºC the high-strength steels loose their strength more rapidly than the low-strength ones, due to the more significant cold-work amount [19].

The approach initially followed in this work, which was already (partially) explored by other researchers, such as Chen and Young [15-17], Ranawaka and Mahendran [21] and Landesmann and Camotim [23-26], consists of modifying Eq. (10) in order to account for the temperature-dependence of $P_{cr.D}$ and P_y. This dependence is felt through the Young's modulus and yield stress values, which are progressively eroded as the temperature (caused by fire conditions) increases. In other words, $P_{cr.D}$ and P_y (or σ_y) are replaced by $P_{cr.D.T}$ and $P_{y.T}$ (or $\sigma_{y.T}$) – note that this approach automatically implies that $\overline{\lambda}_D$ also varies with T.

Figures 5(b) ($T=20$ ºC) and 7 ($T>20$ ºC – elevated temperatures) compare the current DSM distortional strength curve (solid line) with (i) the numerical ultimate loads obtained in this work and (ii) the experimental failure loads reported by Schafer [1], for $T=20$ ºC, and by Ranawaka [19], for $T=100\text{-}200\text{-}500$ ºC. Each plot in Figure 7 concerns a different temperature and the numerical ultimate loads correspond to (i) the lipped channel and rack-section column geometries selected, (ii) five temperature-dependent constitutive models (HR, CF, CY, RM, WJ) and (iii) six room temperature yield stresses ($\sigma_{y.20}=250\text{-}355\text{-}550\text{-}700\text{-}1000\text{-}1200$ *MPa*). On the other hand, Figures 8(a) ($T=20$ ºC) and 9 ($T>20$ ºC) show the corresponding $P_{n.D.T}/P_{u.T}$ *vs.* $\overline{\lambda}_{D.T}$ plots (the numerical values are given in Tables A1 to A7), thus providing pictorial representations of the quality (accuracy and safety) of the current DSM distortional ultimate strength estimates. The observation of the results presented in these seven pairs of figures prompts the following remarks:

(i) At room temperature (Fig. 5(b)), the current DSM strength curve naturally provides accurate and mostly safe predictions of the experimental failure loads reported in [1] – indeed, these experimental failure loads are those used to calibrate this design curve [51, 52]. Concerning the numerical ultimate loads, the DSM estimates are (i_1) safe and accurate for $\overline{\lambda}_D \leq 1.5$ and (i_2) on the unsafe side (but still fairly accurate) in the higher slenderness range – the overestimation tends to grow as $\overline{\lambda}_D$ increases. These assertions are reflected in the average, standard deviation and maximum/minimum values of the numerical $P_{n.D}/P_u$ ratios: *1.02*, *0.08* and *1.13*/*0.85*.

(ii) At elevated temperatures, the modified DSM ultimate strength predictions of the experimental failure loads reported in [19] are (ii_1) safe and fairly accurate for $T=100$ ºC, (ii_2) slightly unsafe for $T=200$ ºC and (ii_3) more unsafe for $T=500$ ºC (particularly if $\overline{\lambda}_D$ is high) – in the last case, the experimental $P_{u.D.T}/P_{y.T}$ values "mingle" quite well with the numerical ones. Concerning the numerical ultimate loads, the DSM estimates are (ii_1) slightly unsafe for $\overline{\lambda}_D \leq 1.5$ and $T<400$ ºC and (ii_2) become progressively more unsafe as $\overline{\lambda}_D$ and/or T increase. In particular, note that they are extremely unsafe for (ii_1) a few stocky columns analysed with the CY model at $T=500\text{-}600$ ºC and (ii_2) most columns analysed with the WJ model at $T=600$ ºC, which is due to the very pronounced yield stress drops prescribed for $T\geq 500$ ºC (CY model) and $T\geq 600$ ºC (WJ model) – in the "WJ columns", which are all quite stocky, the overestimation grows as $\overline{\lambda}_D$ decreases.

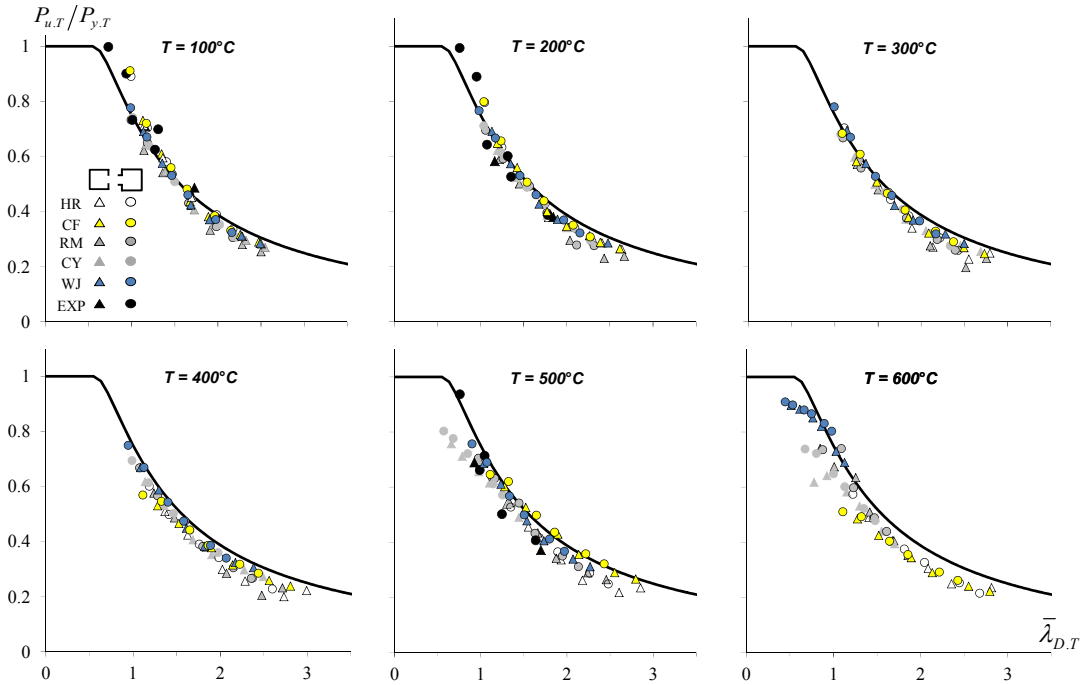

Figure 7: Comparison between the current DSM distortional curve and the column ultimate loads at elevated temperatures.

(iii) At room temperature, there is only two "misaligned" values (P_u/P_y=*0.89*), which correspond to a fairly stocky ($\overline{\lambda}_D$=*0.99*) rack-section column analysed with the HR and CF models – the P_u/P_y values obtained for that same column with the RM, CY and WJ models are considerably lower: *0.73*, *0.77* and *0.80*, respectively. The explanation for this significant discrepancy is certainly due to a combination of several factors, namely (iii$_1$) $\overline{\lambda}_D \approx$*1.00* (practically coincident buckling and squash loads), (iii$_2$) the rather small initial imperfection amplitude and (iii$_3$) the non-negligible differences separating the stress-strain laws prescribed by the five (four) constitutive models in the close vicinity of the transition between the elastic and plastic ranges – see Figure 1(c).

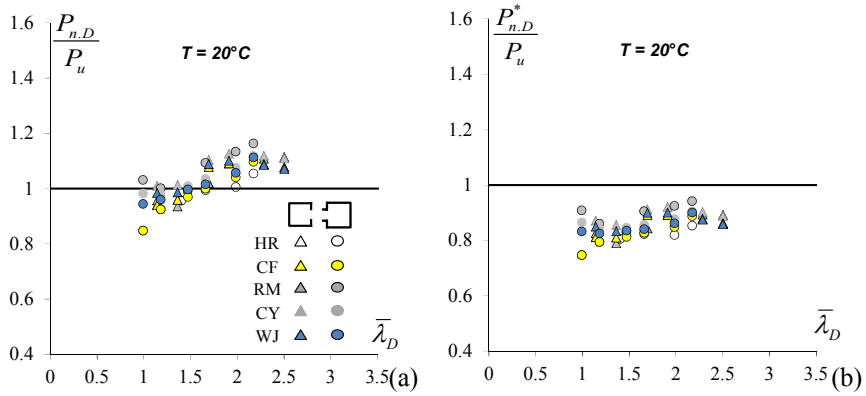

Figure 8: $P_{n.D}/P_u$ and $P^*_{n.D}/P_u$ vs. $\overline{\lambda}_D$ (*T*=*20*°C).

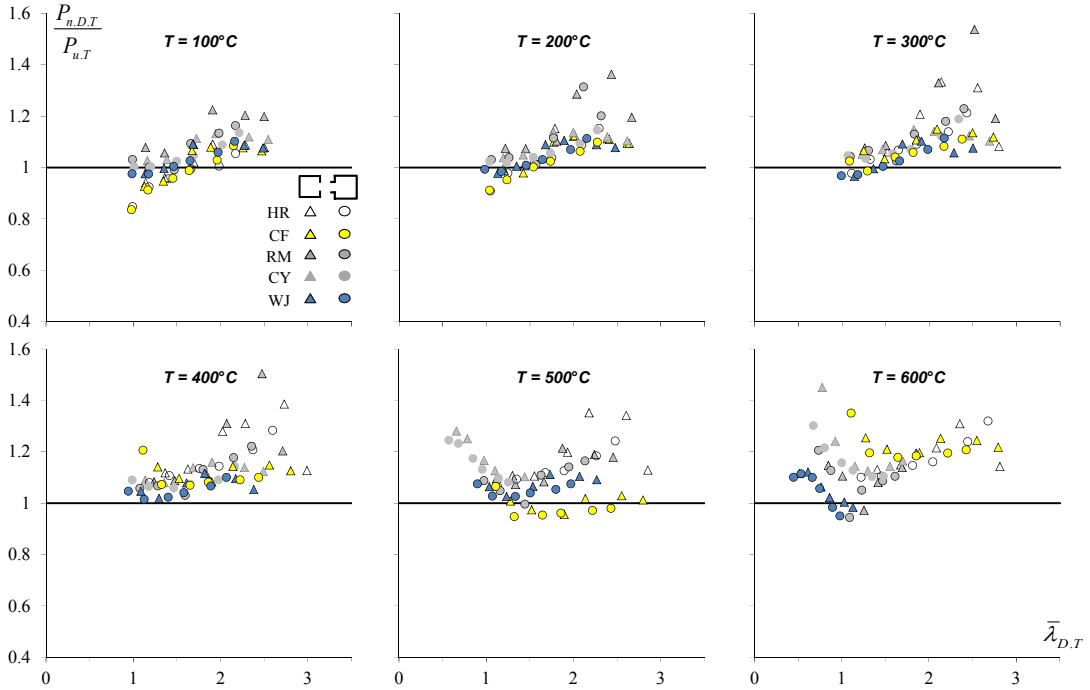

Figure 9: $P_{n.D.T}/P_{u.T}$ vs. $\bar{\lambda}_{D.T}$ ($T>20$ºC).

(iv) Neither the cross-section shape nor the temperature-dependent constitutive model adopted seem to influence visibly the $P_{n.D.T}/P_{u.T}$ "distributions" displayed in Figure 9 (the corresponding values are provided in Tables A2 to A7), whose averages, standard deviations and maximum/minimum values are presented in Figure 10, where $\overline{P}_{n.D.T}$ stands for $P_{n.D.T}/P_{u.T}$. However, there are three exceptions to the above statement, which concern (iv_1) the rather high $P_{n.D.T}/P_{u.T}$ values of the stocky columns analysed with the CY model at T=*500-600* ºC and the WJ model at T=*600* ºC, and (iv_2) the low $P_{n.D.T}/P_{u.T}$ values of the stocky columns analysed with the HR and CF models at T=*100-200*ºC.

(v) The above comparisons show that (v_1) the current (modified) DSM distortional strength curve overestimates the vast majority of numerical column ultimate loads at elevated temperatures, regardless of the temperature-dependent constitutive model adopted, and (v_2) the various "clouds" of $P_{u.D.T}/P_{y.T}$ values remain fairly well "aligned" with Winter-type curves. These facts suggest that a better correlation with the reported numerical column ultimate loads can be achieved by modifying Eq. (10). Therefore, the results of the limited parametric study carried out in this work are used next to develop and propose a (preliminary) alternative design curve, which is obtained by incorporating temperature-dependent parameters into the expressions providing the current DSM distortional strength curve, thus making it possible to predict adequately the ultimate load of columns subjected to elevated temperatures and failing in distortional modes.

6.1 Proposed/alternative DSM distortional strength curves

On the basis of the ultimate strength data gathered in the limited parametric study presented earlier, a first attempt was made to find a unified DSM design approach aimed at predicting efficiently (safely and economically) the numerical failure loads concerning the columns analysed at all temperature values. The outcome of this effort is the proposal of the alternative DSM distortional design curve defined by

$$P^{*}_{n.D.T} = \begin{cases} P_{y.T} & \text{for } \bar{\lambda}_{D.T} \le c \\ P_{y.T}\left[a - 0.15\left(P_{cr.D.T}/P_{y.T}\right)^{b}\right]\left(P_{cr.D.T}/P_{y.T}\right)^{b} & \text{for } \bar{\lambda}_{D.T} > c \end{cases} , \quad (11)$$

which was obtained by modifying Eq. (10) as follows: (i) the coefficient *0.25* was replaced by *0.15* and (ii) three (slightly) temperature-dependent parameters (*a*, *b*, *c*) were incorporated, replacing the coefficient *1*, power *0.6* and transition distortional value *0.561*, respectively. The parameter values adopted, namely (i) *a=0.81*, *b=0.62* and *c=0.594* (*T*≤ *300* ºC) or (ii) *a=0.79*, *b=0.66* and *c=0.567* (*T* >*300* ºC), ensure mostly safe (but not excessively so) DSM failure load estimates for all the temperatures (including *T=20* ºC) considered in this work, as can be visually confirmed by looking at Figures 5(b) (*T=20* ºC) and 10 (*T* >*20* ºC), which make it possible to compare the proposed DSM distortional strength curves with (i) the current ones, defined in Eq. (10), and (ii) the numerical and experimental column ultimate load. Moreover, Figures 8(b) (*T=20* ºC) and 11 (*T>20* ºC) plot the variation of $P^{*}_{n.D.T}/P_{u.T}$ values with $\bar{\lambda}_{D.T}$ – all the $P^{*}_{n.D.T}$ predictions are given in Tables A1 to A7, together with the corresponding averages, standard deviations and maximum/minimum values. The close observation of the results presented in all these figures leads to the following conclusions:

(i) Despite the inherent simplicity of the modifications, the proposed (preliminary) DSM distortional strength curves provide fairly satisfactory ultimate load estimates for most of the columns analysed: lipped channel and rack-section columns exhibiting five temperature-dependent steel constitutive models and subjected to seven temperatures. Indeed, the averages and standard deviations of the numerical $P^{*}_{n.D.T}/P_{u.T}$ values vary from (i_1) *0.86* (*T=20* ºC) to *0.94* (*T=600* ºC), and (i_2) *0.04* (*T=20* ºC) to *0.11* (*T=500* ºC).

(ii) The averages and standard deviations of the numerical $P_{n.D}/P_{u.T}$ values (current DSM curve) are clearly "worse" (particularly the former): they vary from (ii_1) *1.03* (*T=20* ºC) to *1.17* (*T=400-600* ºC), and (ii_2) *0.07* (*T=20* ºC) to *0.11* (*T=300* ºC).

(iii) Nevertheless, practically all the failure loads of the stocky lipped channel and rack-section columns analysed with (iii_1) the CY model at *T=500-600* ºC and (iii_2) the WJ model at *T=600* ºC are still considerably overestimated by the propose strength curves, *i.e.*, the corresponding ultimate load erosion is not yet adequately captured.

(iv) The $P^{*}_{n.D.T}$ values provide safe estimates for all experimental column ultimate loads.

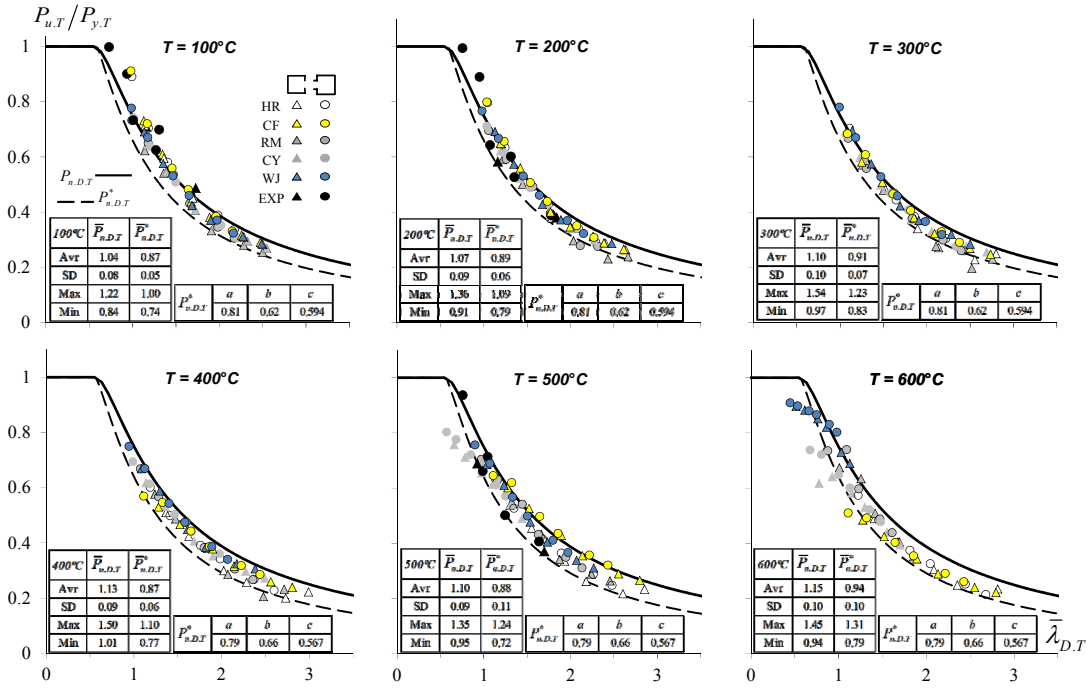

Figure 10: Comparison between the proposed/alternative DSM estimates and the numerical/experimental column ultimate loads ($T \geq 100$ ºC).

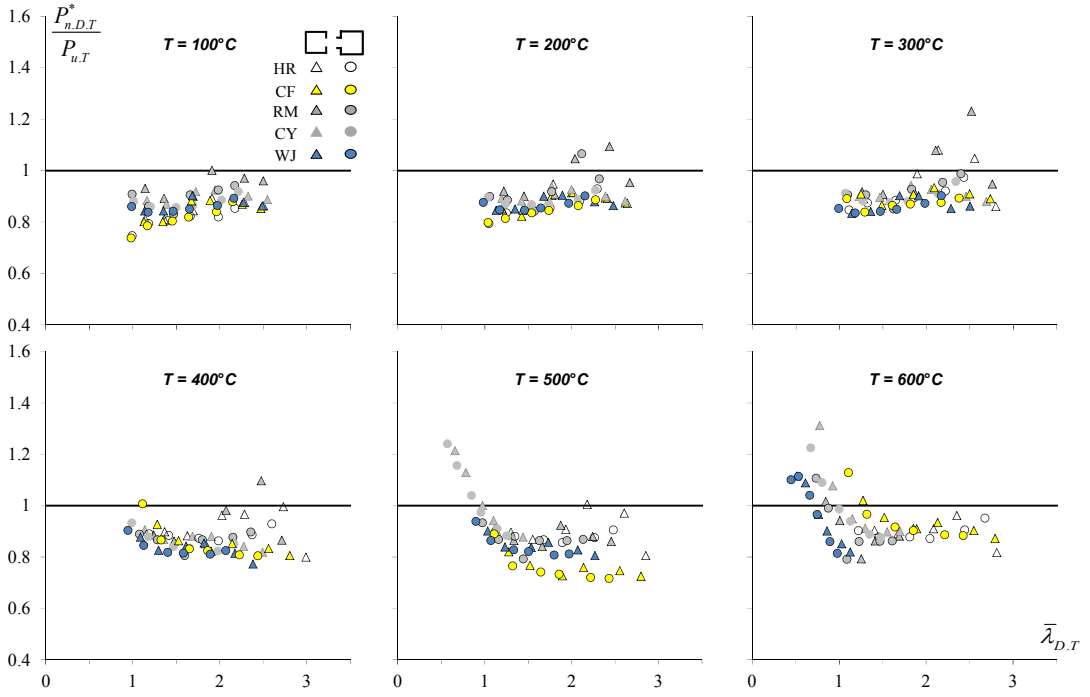

Figure 11: Variation of $P^*_{n.D.T}/P_{u.T}$ with $\bar{\lambda}_{D.T}$ for the six elevated temperatures (numerical).

Finally, Figure 12 compares the two proposed/alternative DSM distortional strength curves (for $T \leq 300$ ºC and $T > 300$ ºC) with the current one, developed for room temperature ($T=20$ ºC). Since the transition distortional values are very close (*0.561*, *0.597*, *0.567*), the curves differ essentially in their descending branches. Moreover, one readily observes that the two proposed curves (i) lie clearly below the current one and (ii) practically coincide for $\overline{\lambda}_D \leq 1.00$ – this coincidence explains why the $T > 300$ ºC strength curve is not able to capture the strong ultimate strength erosion occurring for the stocky columns analysed with the CY (mostly) and WJ models and subjected to the higher temperatures ($T=500$-600 ºC).

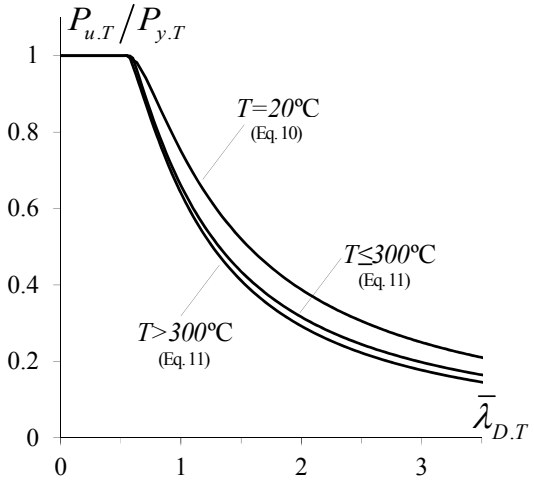

Figure 12: Comparison between the current (room temperature) and proposed (elevated temperatures) DSM distortional strength curves.

7 Conclusion

This paper reports a numerical (ANSYS SFEA) investigation aimed at assessing the performance of the current DSM distortional strength curve to estimate the failure loads of fixed-ended cold-formed steel lipped channel and rack-section columns (i) subjected to various uniform temperature distributions (up to *600* ºC) caused by fire conditions, (ii) exhibiting several room-temperature yield stresses, selected to cover a wide distortional slenderness range, and (iii) displaying five different temperature-dependent steel stress-strain laws, namely the models prescribed in EC3-1.2 for hot-rolled and cold-formed steel grades and the experimentally-based proposals due to Chen and Young [16], Ranawaka and Mahendran [20], and Wei and Jihong [34]. The focus of the work was precisely to quantify the quality (accuracy and safety) of the current DSM distortional ultimate load predictions and to appraise how that quality was affected by the particular temperature-dependent steel constitutive model adopted. These goals were achieved by comparing numerical distortional failure load data, obtained by means of non-linear SFEA incorporating small-amplitude critical-mode initial imperfections and involving *420* columns, with their current DSM estimates – a few experimental column failure loads reported by Ranawaka [19]

were also included in the comparison. The output of this comparison also led to the proposal of a few alternative (slightly modified) DSM strength curves to enable a more adequate capture of the elevated temperature effects.

Out of the various findings unveiled in this work, the following deserve a special mention:

(i) The $P_{u.T}/P_{y.T}$ *vs.* $\overline{\lambda}_{D.T}$ "clouds" concerning the numerical ultimate loads obtained with the five temperature-dependent steel constitutive model were shown to follow trends that can be accurately described by "Winter-type" strength/design curves (the few experimental distortional failure loads available in the literature also followed a similar trend). Moreover, the "vertical dispersion" was found to be perfectly acceptable for all of them, with two exceptions: the stocky columns subjected to $T=600$ ºC and analysed with the models proposed by of Chen and Young [16] and Wei and Jihong [34].

(ii) The $P_{u.T}/P_{y.T}$ values of the columns at room temperature ($T=20$ ºC) or subjected to $T=100$ ºC were above those concerning the columns subjected to elevated temperatures ($T>100$ ºC). This statement is also valid for the few experimental failure loads available.

(iii) The current DSM distortional ultimate strength estimates were found (iii_1) to be slightly (acceptably) unsafe for $\overline{\lambda}_D \leq 1.5$ and $T<400$ ºC, (iii_2) to became gradually more unsafe as $\overline{\lambda}_D$ and/or T increase and (iii_3) to be too unsafe for stocky columns analysed with the models of (iii_1) Chen and Young ($T=500$-600 ºC) and (iii_1) Wei and Jihong ($T=600$ ºC).

(iv) A first attempt was made to find a DSM design approach to predict efficiently the numerical distortional failure loads of all the columns analysed, regardless of the cross-section shape, temperature value and/or steel constitutive model. It consisted of incorporating three (slightly) temperature-dependent parameters into the current DSM distortional strength expressions – different values for $T \leq 300$ ºC and $T>300$ ºC. In spite of the inherent simplicity of these changes, the ensuing DSM distortional strength curves were shown to predict fairly well the vast majority of the numerical and experimental column distortional failure loads.

(v) Indeed, the proposed/modified predicted-to-numerical ultimate load ratio averages and standard deviations are in the ranges *0.86-0.94* and *0.04-0.11* for all the temperatures – the same intervals for their current DSM counterparts are *1.03-1.17* and *0.07-0.11*.

(vi) It seems fair to say that, on the basis of the limited amount of results reported in this work, an adequate answer to the question "how relevant is the temperature-dependence of the material behaviour?" is "not too much", as the conclusions drawn from this study apply quite similarly to the five temperature-dependent constitutive models considered.

The authors are plan to extend the scope of this investigation to cover additional (i) column geometries (cross-section shape/dimensions and lengths) and (ii) available temperature-dependent constitutive models. Furthermore, since only a few numerical results were presented for stocky columns subjected to high temperatures

(*T=500-600*ºC), more data should be obtained for on this slenderness range, in order to either confirm or supplement the findings reported in this work.

References

[1] B.W. Schafer, "Review: the Direct Strength Method of cold-formed steel member design", *Journal of Constructional Steel Research*, **64**(7-8), 766-88, 2008.

[2] American Iron and Steel Institute (AISI), *North American Specification for the Design of Cold-Formed Steel Structural Members* – – NAS: AISI-S100-07, Washington (DC), 2007.

[3] Standards of Australia and Standards of New Zealand (SA-SNZ), *Australian/New Zealand Standard on Cold-Formed Steel Structures* – AS/NZS 4600 (2nd edition), Sydney-Wellington, 2005.

[4] Brazilian Standards Association (ABNT), *Brazilian Standard on Design of Cold-Formed Steel Structures* – NBR 14762:2010, Rio de Janeiro, RJ, 2010. (Portuguese)

[5] J. Outinen, O. Kaitila, P. Makeläinen, "A study for the development of the design of steel structures in fire conditions", *Proceedings of First International Workshop on Structures in Fire* (SIF'2000 – Copenhagen, 19-20/6), J.M. Franssen (ed.), 267-281.

[6] O. Kaitila, "Imperfection sensitivity analysis of lipped channel columns at high temperatures", *Journal of Constructional Steel Research*, **58**(3), 333-51.

[7] M. Feng, Y.C. Wang, J.M. Davies, "Structural behaviour of cold-formed thin-walled short steel channel columns at elevated temperatures − Part 1: Experiments", *Thin-Walled Structures*, **41**(6), 543-70, 2003.

[8] M. Feng, Y.C. Wang, J.M. Davies, "Structural behaviour of cold-formed thin-walled short steel channel columns at elevated temperatures − Part 2: Design calculations and numerical analysis", *Thin-Walled Structures*, **41**(6), 571-94, 2003.

[9] M. Feng, Y.C. Wang, J.M. Davies, "Thermal performance of cold-formed thin-walled steel panel systems in fire", *Fire Safety Journal*, **38**(4), 365-94, 2003.

[10] M. Feng, Y.C. Wang, J.M. Davies, "Axial strength of cold-formed thin-walled steel channels under non-uniform temperatures in fire", *Fire Safety Journal*, **38**(8), 679-707, 2003.

[11] M. Feng, Y.C. Wang, J.M. Davies, "A numerical imperfection sensitivity study of cold-formed thin-walled tubular steel columns at uniform elevated temperatures", *Thin-Walled Structures*, **42**(4), 533-55, 2004.

[12] J.H. Lee, M. Mahendran, P. Makeläinen, "Prediction of mechanical properties of light gauge steels at elevated temperatures", *Journal of Constructional Steel Research*, **59**(12), 1517-32, 2003.

[13] M. Feng, Y.C. Wang, "An analysis of the structural behaviour of axially loaded full-scale cold-formed thin-walled steel structural panels tested under fire conditions", *Thin-Walled Structures*, **43**(2), 291-332, 2005.

[14] M. Feng, Y.C. Wang, "An experimental study of loaded full-scale cold-formed thin-walled steel structural panels under fire conditions, *Fire Safety Journal*, **40**(1), 43-63, 2005.
[15] J. Chen, B. Young, "Corner properties of cold-formed steel sections at elevated temperatures", *Thin-Walled Structures*, **44**(2), 216-23, 2006.
[16] J. Chen, B. Young, "Experimental investigation of cold-formed steel material at elevated temperatures", *Thin-Walled Structures*, **45**(1), 96-110, 2007.
[17] J. Chen, B. Young, "Cold-formed steel lipped channel columns at elevated temperatures", *Engineering Structures*, **29**(10), 2445-56, 2007.
[18] J. Chen, B. Young, "Design of high strength steel columns at elevated temperatures", *Journal of Constructional Steel Research*, **64**(6), 689-703, 2008.
[19] T. Ranawaka, *Distortional Buckling Behaviour of Cold-Formed Steel Compression Members at Elevated Temperatures*, Ph.D. Thesis in Civil Engineering, Queensland University of Technology, Brisbane, Australia, 2006.
[20] T. Ranawaka, M. Mahendran, "Experimental study of the mechanical properties of light gauge cold-formed steels at elevated temperatures", *Fire Safety Journal*, **44**(2), 219–29, 2009.
[21] T. Ranawaka, M. Mahendran, "Distortional buckling tests of cold-formed steel compression members at elevated temperatures", *Journal of Constructional Steel Research*, **65**(2), 249-59, 2009.
[22] T. Ranawaka, M. Mahendran, "Numerical modelling of light gauge cold-formed steel compression members subjected to distortional buckling at elevated temperatures", *Thin-Walled Structures*, **48**(3-4), 334-44, 2010.
[23] A. Landesmann, D. Camotim, "Distortional failure and design of cold-formed steel lipped channel columns under fire conditions", *Proceedings of SSRC Annual Stability Conference* (Orlando, 12-15/5), 505-532, 2010.
[24] A. Landesmann, D. Camotim D, "Distortional failure and design of cold-formed steel rack-section columns under fire conditions", *Proceedings of Fourth International Conference on Steel & Composite Structures* (ICSCS'2011 – Sydney, 21-23/7), B. Uy *et al.* (eds.), 287-289, 2011. (full paper in CD-ROM Proceedings)
[25] A. Landesmann, D. Camotim, "On the distortional buckling, post-buckling and strength of cold-formed steel lipped channel columns under fire conditions", *Journal of Structural Fire Engineering*, **2**(1), 1-19, 2011.
[26] A. Landesmann, D. Camotim, "DSM design of cold-formed steel columns failing distortionally exposed to fire: how relevant is the temperature dependence of the material behavior?", *USB Proceedings of the SSRC Annual Stability Conference* (Grapevine, 18-21/4), 2012.
[27] A. Shahbazian, Y.C. Wang, "Calculating the global buckling resistance of thin-walled steel members with uniform and non-uniform elevated temperatures under axial compression", *Thin-Walled Structures*, **49**(11), 1415-28, 2011.
[28] A. Shahbazian, Y.C. Wang, "Application of the Direct Strength Method to local buckling resistance of thin-walled steel members with non-uniform

elevated temperatures under axial compression", *Thin-Walled Structures*, **49**(12), 1573-83, 2011.

[29] A. Shahbazian, Y.C. Wang, "Direct Strength Method for calculating distortional buckling capacity of cold-formed thin-walled steel columns with uniform and non-uniform elevated temperatures", *Thin-Walled Structures*, **53**(April), 188-99, 2012.

[30] J. Outinen, P. Makeläinen, "Mechanical properties of structural steel at elevated temperatures", *Proceedings of Third International Conference on Advances in Steel Structures* (ICASS'2002 – Hong Kong, 9-11/12), S.L. Chan, J.G. Teng, K.F. Chung (eds.), 1103-1110, 2002.

[31] E. Mecozzi, B. Zhao, "Development of stress-strain relationships of cold-formed lightweight steel at elevated temperatures", *Proceedings of Fourth European Conference on Steel and Composite Structures* (EUROSTEEL'2005 – Maastricht, 8-10/6) B. Hoffmeister, O. Hechler (eds.), 5.1/41-49 (vol. C), 2005.

[32] B. Zhao, J. Kruppa, C. Renaud, M. O'Connor, E. Mecozzi, *Calculation Rules of Lightweight Steel Sections in Fire Situations*, EUR-21426 (Technical Steel Research Series) – Steel Products and Applications for Building, Construction and Industry, European Commission Technical Steel Research, Luxembourg, 2005.

[33] N.D. Kankanamge, M. Mahendran, "Mechanical properties of cold-formed steels at elevated temperatures", *Thin-Walled Structures*, **49**(1), 26-44, 2011.

[34] C. Wei, Y. Jihong, "Mechanical properties of G550 cold-formed steel under transient and steady state conditions", *Journal of Constructional Steel Research*, **73**(June), 1-11, 2012.

[35] Swanson Analysis Systems Inc. (SAS), *ANSYS Reference Manual* (vrs. 12), 2009.

[36] M.P. Sidey, D.P. Teague, *Elevated Temperature Data for Structural Grades of Galvanised Steel*, British Steel Report, Welsh Laboratories, UK, 1988.

[37] British Standards Institution (BSI), *Structural Use of Steelwork in Building – Part 8: Code of Practice for Fire Resistance Design* – BS5950-8, London, 1990.

[38] Comité Européen de Normalisation (CEN), *Eurocode 3: Design of Steel Structures – Part 1-2: General Rules – Structural Fire Design* – EC3-1.2, Brussels, 2005.

[39] B.R. Kirby, R.R. Preston, "High temperatures properties of hot-rolled structural steels for use in fire engineering design studies", *Fire Safety Journal*, **13**(1), 27-37, 1988.

[40] W. Ramberg, W.R. Osgood, *Description of Stress-Strain Curves by Three Parameters*, NACA Technical Note 902, 1943.

[41] E. Mirambell, E. Real, "On the calculation of deflections in structural stainless steel beams: an experimental and numerical investigation", *Journal of Constructional Steel Research*, **54**(1), 109-33, 2000.

[42] K.J.R. Rasmussen, "Full-range stress-strain curves for stainless steel alloys", *Journal of Constructional Steel Research*, **59**(1), 47-61, 2003.

[43] J. Outinen, *Mechanical Properties of Structural Steels at Elevated Temperatures*, Licentiate Thesis, Helsinki University of Technology, Finland, 1999.

[44] R. Bebiano, P. Pina, N. Silvestre, D. Camotim, *GBTUL 1.0β – Buckling and Vibration Analysis of Thin-Walled Members*, DECivil/IST, Technical University of Lisbon, Portugal, 2008. (http://www.civil.ist.utl.pt/gbt)

[45] R. Bebiano, N. Silvestre, D. Camotim, "GBTUL – A code for the buckling analysis of cold-formed steel members", *Proceedings of 19th International Specialty Conference on Recent Research and Developments in Cold-Formed Steel Design and Construction* (St. Louis, 14-15/10), R. LaBoube, W.W. Yu (eds.), 61-79, 2008.

[46] A. Landesmann, D. Camotim, E.M. Batista, "On the distortional buckling, post-buckling and strength of cold-formed steel lipped channel columns subjected to elevated temperatures", *Proceedings of International Conference on Applications of Structural Fire Engineering* (Prague), F. Wald, P. Kallerová, J. Chlouba (eds.), A8-A13, 2009.

[47] L.C. Prola, D. Camotim, "On the distortional post-buckling behaviour of cold-formed lipped channel steel columns", *Proceedings of SSRC Annual Stability Conference* (Seattle, 24-27/4), 571-590, 2002.

[48] L.C. Prola, D. Camotim, "On the Distortional Post-Buckling Behaviour of Rack-Section Cold-Formed Steel Columns", in B.H.V. Topping, Z. Bittnar, (Editors), "Proceedings of the Sixth International Conference on Computational Structures Technology", Civil-Comp Press, Stirlingshire, UK, Paper 98, 2002. doi:10.4203/ccp.75.98

[49] G.J. Hancock, Y.B. Kwon, E.S. Bernard, "Strength design curves for thin-walled sections undergoing distortional buckling", *Journal of Constructional Steel Research*, **31**(2-3), 169-186, 1994.

[50] B.W. Schafer, T. Peköz, "Direct strength prediction of cold-formed steel members using numerical elastic buckling solutions", *Proceedings of 14th International Specialty Conference on Cold-formed Steel Structures* (St. Louis, 15-16/10), R. LaBoube, W.-W. Yu (eds.), 69-76, 1998.

[51] B.W. Schafer, *Distortional Buckling of Cold-Formed Steel Columns*, American Iron and Steel Institute (AISI) Report, Washington DC, 2000.

[52] B.W. Schafer, *Direct Strength Method Design Guide*, American Iron and Steel Institute (AISI) Report, Washington DC, 2005.

Annex

Tables A1 (room temperature) and A2-A7 (elevated temperatures) summarise the numerical (ANSYS SFEA) column ultimate strengths and the corresponding DSM estimates obtained in the course of this investigation. Each table concerns the two column geometries (C130 and R135, identified as Part I and Part II, respectively) and provides information about (i) the steel material model, including the corresponding k_y and k_e values for the temperatures considered (no other reduction factor is given), (ii) the column critical (distortional) buckling loads P_{cr}, as well as the corresponding slenderness values $\overline{\lambda}_D$, (iii) the squash (P_y) and failure/ultimate (P_u) loads, as well as the ratios between them (P_u/P_y), (iv) the ultimate strength estimates provided by the current/modified ($P_{n.D}$) and proposed ($P^*_{n.D}$) DSM strength curves, as well as the ratios $P_{n.D}/P_y$ and $P^*_{n.D}/P_y$, and (v) the predicted-to-numerical ultimate load ratios $P_{n.D}/P_u$ and $P^*_{n.D}/P_u$.

σ-ε	k_y	k_e	P_{cr} (kN)	$\bar{\lambda}_D$	P_y (kN)	P_u (kN)	$P_{n.D}$ (kN)	$\frac{P_u}{P_y}$	$\frac{P_{n.D}}{P_y}$	$\frac{P_{n.D}}{P_u}$	$P^*_{n.D}$ (kN)	$\frac{P^*_{n.D}}{P_y}$	$\frac{P^*_{n.D}}{P_u}$
HR	1.000	1.000	135.97	1.14	177.5	126.5	119.0	0.71	0.67	0.94	102.7	0.58	0.81
				1.36	252.1	150.0	144.0	0.60	0.57	0.96	121.7	0.48	0.81
				1.69	390.5	176.1	179.8	0.45	0.46	1.02	148.6	0.38	0.84
				1.91	497.0	185.3	202.1	0.37	0.41	1.09	165.3	0.33	0.89
				2.29	710.0	219.7	238.9	0.31	0.34	1.09	192.7	0.27	0.88
				2.50	852.0	241.1	259.7	0.28	0.30	1.08	208.1	0.24	0.86
CF	1.000	1.000	135.97	1.14	177.5	126.7	119.0	0.71	0.67	0.94	102.7	0.58	0.81
				1.36	252.1	150.2	144.0	0.60	0.57	0.96	121.7	0.48	0.81
				1.69	390.5	166.8	179.8	0.43	0.46	1.08	148.6	0.38	0.89
				1.91	497.0	185.2	202.1	0.37	0.41	1.09	165.3	0.33	0.89
				2.29	710.0	219.5	238.9	0.31	0.34	1.09	192.7	0.27	0.88
				2.50	852.0	241.4	259.7	0.28	0.30	1.08	208.1	0.24	0.86
WJ	1.000	1.000	135.97	1.14	177.5	121.0	119.0	0.68	0.67	0.98	102.7	0.58	0.85
				1.36	252.1	146.0	144.0	0.58	0.57	0.99	121.7	0.48	0.83
				1.69	390.5	165.2	179.8	0.42	0.46	1.09	148.6	0.38	0.90
				1.91	497.0	183.6	202.1	0.37	0.41	1.10	165.3	0.33	0.90
				2.29	710.0	220.2	238.9	0.31	0.34	1.09	192.7	0.27	0.88
				2.50	852.0	242.5	259.7	0.28	0.30	1.07	208.1	0.24	0.86
RM	1.000	1.000	135.97	1.14	177.5	124.4	119.0	0.70	0.67	0.96	102.7	0.58	0.83
				1.36	252.1	154.0	144.0	0.61	0.57	0.94	121.7	0.48	0.79
				1.69	390.5	176.3	179.8	0.45	0.46	1.02	148.6	0.38	0.84
				1.91	497.0	185.4	202.1	0.37	0.41	1.09	165.3	0.33	0.89
				2.29	710.0	215.6	238.9	0.30	0.34	1.11	192.7	0.27	0.89
				2.50	852.0	233.2	259.7	0.27	0.30	1.11	208.1	0.24	0.89
CY	1.000	1.000	135.97	1.14	177.5	117.9	119.0	0.66	0.67	1.01	102.7	0.58	0.87
				1.36	252.1	142.1	144.0	0.56	0.57	1.01	121.7	0.48	0.86
				1.69	390.5	162.9	179.8	0.42	0.46	1.10	148.6	0.38	0.91
				1.91	497.0	179.5	202.1	0.36	0.41	1.13	165.3	0.33	0.92
				2.29	710.0	213.5	238.9	0.30	0.34	1.12	192.7	0.27	0.90
				2.50	852.0	234.0	259.7	0.27	0.30	1.11	208.1	0.24	0.89

Table A1 – Part I: Numerical ultimate loads and DSM estimates – *C130* columns analysed at *20*ºC.

σ-ε	k_y	k_e	P_{cr} (kN)	$\bar{\lambda}_D$	P_y (kN)	P_u (kN)	$P_{n.D}$ (kN)	$\frac{P_u}{P_y}$	$\frac{P_{n.D}}{P_y}$	$\frac{P_{n.D}}{P_u}$	$P^*_{n.D}$ (kN)	$\frac{P^*_{n.D}}{P_y}$	$\frac{P^*_{n.D}}{P_u}$
HR	1.000	1.000	256.21	0.99	252.5	224.8	190.5	0.89	0.75	0.85	167.8	0.66	0.75
				1.18	358.6	252.3	233.2	0.70	0.65	0.92	200.3	0.56	0.79
				1.40	505.0	293.1	280.2	0.58	0.55	0.96	235.9	0.47	0.80
				1.66	707.0	334.3	332.2	0.47	0.47	0.99	275.1	0.39	0.82
				1.99	1010.0	392.8	394.8	0.39	0.39	1.01	321.9	0.32	0.82
				2.17	1212.0	408.0	430.1	0.34	0.35	1.05	348.1	0.29	0.85
CF	1.000	1.000	256.21	0.99	252.5	224.8	190.5	0.89	0.75	0.85	167.8	0.66	0.75
				1.18	358.6	252.3	233.2	0.70	0.65	0.92	200.3	0.56	0.79
				1.47	555.5	303.6	294.3	0.55	0.53	0.97	246.6	0.44	0.81
				1.66	707.0	332.5	332.2	0.47	0.47	1.00	275.1	0.39	0.83
				1.99	1010.0	379.5	394.8	0.38	0.39	1.04	321.9	0.32	0.85
				2.17	1212.0	392.3	430.1	0.32	0.35	1.10	348.1	0.29	0.89
WJ	1.000	1.000	256.21	0.99	252.5	201.7	190.5	0.80	0.75	0.94	167.8	0.66	0.83
				1.18	358.6	243.0	233.2	0.68	0.65	0.96	200.3	0.56	0.82
				1.47	555.5	295.3	294.3	0.53	0.53	1.00	246.6	0.44	0.83
				1.66	707.0	327.3	332.2	0.46	0.47	1.02	275.1	0.39	0.84
				1.99	1010.0	373.6	394.8	0.37	0.39	1.06	321.9	0.32	0.86
				2.17	1212.0	386.7	430.1	0.32	0.35	1.11	348.1	0.29	0.90
RM	1.000	1.000	256.21	0.99	252.5	184.5	190.5	0.73	0.75	1.03	167.8	0.66	0.91
				1.18	358.6	232.6	233.2	0.65	0.65	1.00	200.3	0.56	0.86
				1.47	555.5	296.8	294.3	0.53	0.53	0.99	246.6	0.44	0.83
				1.66	707.0	303.6	332.2	0.43	0.47	1.09	275.1	0.39	0.91
				1.99	1010.0	347.9	394.8	0.34	0.39	1.13	321.9	0.32	0.93
				2.17	1212.0	369.5	430.1	0.30	0.35	1.16	348.1	0.29	0.94
CY	1.000	1.000	256.21	0.99	252.5	194.1	190.5	0.77	0.75	0.98	167.8	0.66	0.86
				1.18	358.6	238.1	233.2	0.66	0.65	0.98	200.3	0.56	0.84
				1.47	555.5	291.6	294.3	0.52	0.53	1.01	246.6	0.44	0.85
				1.66	707.0	321.2	332.2	0.45	0.47	1.03	275.1	0.39	0.86
				1.99	1010.0	367.0	394.8	0.36	0.39	1.08	321.9	0.32	0.88
				2.17	1212.0	384.9	430.1	0.32	0.35	1.12	348.1	0.29	0.90

Table A1 – Part II: Numerical ultimate loads and DSM estimates – *R135* columns analysed at *20*ºC.

σ-ε	k_y	k_e	P_{cr} (kN)	$\bar{\lambda}_D$	P_y (kN)	P_u (kN)	$P_{n.D}$ (kN)	$\frac{P_u}{P_y}$	$\frac{P_{n.D}}{P_y}$	$\frac{P_{n.D}}{P_u}$	$P^*_{n.D}$ (kN)	$\frac{P^*_{n.D}}{P_y}$	$\frac{P^*_{n.D}}{P_u}$
HR	1.000	1.000	135.97	1.14	177.5	126.5	119.0	0.71	0.67	0.94	102.7	0.58	0.81
				1.36	252.1	150.0	144.0	0.60	0.57	0.96	121.7	0.48	0.81
				1.69	390.5	176.1	179.8	0.45	0.46	1.02	148.6	0.38	0.84
				1.91	497.0	185.3	202.1	0.37	0.41	1.09	165.3	0.33	0.89
				2.29	710.0	219.7	238.9	0.31	0.34	1.09	192.7	0.27	0.88
				2.50	852.0	241.1	259.7	0.28	0.30	1.08	208.1	0.24	0.86
CF	0.977	1.000	135.97	1.13	173.4	126.7	117.5	0.73	0.68	0.93	101.6	0.59	0.80
				1.35	246.3	150.2	142.2	0.61	0.58	0.95	120.3	0.49	0.80
				1.68	381.5	166.8	177.8	0.44	0.47	1.07	147.1	0.39	0.88
				1.89	485.6	185.2	199.9	0.38	0.41	1.08	163.6	0.34	0.88
				2.26	693.7	219.5	236.4	0.32	0.34	1.08	190.8	0.28	0.87
				2.47	832.4	241.4	257.0	0.29	0.31	1.06	206.1	0.25	0.85
WJ	0.987	0.998	135.70	1.14	175.2	121.0	118.1	0.69	0.67	0.98	102.0	0.58	0.84
				1.35	248.8	143.3	142.9	0.58	0.57	1.00	120.8	0.49	0.84
				1.69	385.4	163.5	178.5	0.42	0.46	1.09	147.6	0.38	0.90
				1.90	490.5	181.8	200.7	0.37	0.41	1.10	164.2	0.33	0.90
				2.27	700.8	218.5	237.3	0.31	0.34	1.09	191.4	0.27	0.88
				2.49	840.9	239.7	257.9	0.29	0.31	1.08	206.7	0.25	0.86
RM	0.998	1.000	135.97	1.14	177.1	110.3	118.9	0.67	1.08	1.08	102.6	0.58	0.93
				1.36	251.5	136.1	143.8	0.57	1.06	1.06	121.5	0.48	0.89
				1.69	389.7	164.9	179.7	0.46	1.09	1.09	148.5	0.38	0.90
				1.91	496.0	164.9	201.9	0.41	1.22	1.22	165.1	0.33	1.00
				2.28	708.6	198.4	238.7	0.34	1.20	1.20	192.5	0.27	0.97
				2.50	850.3	216.5	259.5	0.31	1.20	1.20	207.9	0.24	0.96
CY	0.972	0.938	127.54	1.16	172.5	111.0	113.9	0.66	1.03	1.03	98.1	0.57	0.88
				1.39	245.0	133.5	137.6	0.56	1.03	1.03	116.0	0.47	0.87
				1.73	379.6	154.2	171.7	0.45	1.11	1.11	141.6	0.37	0.92
				1.95	483.1	170.4	192.8	0.40	1.13	1.13	157.5	0.33	0.92
				2.33	690.1	203.6	227.8	0.33	1.12	1.12	183.5	0.27	0.90
				2.55	828.1	223.2	247.6	0.30	1.11	1.11	198.1	0.24	0.89

Table A2 – Part I: Numerical ultimate loads and DSM estimates – *C130* columns analysed at *100*ºC.

σ-ε	k_y	k_e	P_{cr} (kN)	$\bar{\lambda}_D$	P_y (kN)	P_u (kN)	$P_{n.D}$ (kN)	$\frac{P_u}{P_y}$	$\frac{P_{n.D}}{P_y}$	$\frac{P_{n.D}}{P_u}$	$P^*_{n.D}$ (kN)	$\frac{P^*_{n.D}}{P_y}$	$\frac{P^*_{n.D}}{P_u}$
HR	1.000	1.000	256.21	0.99	252.5	224.8	190.5	0.75	0.85	0.85	167.8	0.66	0.75
				1.18	358.6	252.3	233.2	0.65	0.92	0.92	200.3	0.56	0.79
				1.40	505.0	293.1	280.2	0.55	0.96	0.96	235.9	0.47	0.80
				1.66	707.0	334.3	332.2	0.47	0.99	0.99	275.1	0.39	0.82
				1.99	1010.0	392.8	394.8	0.39	1.01	1.01	321.9	0.32	0.82
				2.17	1212.0	408.0	430.1	0.35	1.05	1.05	348.1	0.29	0.85
CF	0.977	1.000	256.21	0.98	246.7	224.8	187.8	0.76	0.84	0.84	165.8	0.67	0.74
				1.17	350.3	252.3	230.2	0.66	0.91	0.91	198.1	0.57	0.79
				1.46	542.7	303.6	290.8	0.54	0.96	0.96	243.9	0.45	0.80
				1.64	690.7	332.5	328.4	0.48	0.99	0.99	272.2	0.39	0.82
				1.96	986.8	379.5	390.5	0.40	1.03	1.03	318.6	0.32	0.84
				2.15	1184.1	392.3	425.5	0.36	1.08	1.08	344.7	0.29	0.88
WJ	0.987	0.998	255.70	0.99	249.2	193.6	188.8	0.76	0.98	0.98	166.5	0.67	0.86
				1.18	353.9	237.3	231.3	0.65	0.97	0.97	198.9	0.56	0.84
				1.46	548.3	290.9	292.0	0.53	1.00	1.00	244.8	0.45	0.84
				1.65	697.8	321.3	329.8	0.47	1.03	1.03	273.2	0.39	0.85
				1.97	996.9	370.0	392.0	0.39	1.06	1.06	319.7	0.32	0.86
				2.16	1196.2	387.5	427.0	0.36	1.10	1.10	345.8	0.29	0.89
RM	0.998	1.000	256.21	0.99	252.0	184.5	190.3	0.75	1.03	1.03	167.6	0.67	0.91
				1.18	357.8	232.6	232.9	0.65	1.00	1.00	200.2	0.56	0.86
				1.47	554.4	296.8	294.0	0.53	0.99	0.99	246.3	0.44	0.83
				1.66	705.6	303.6	331.9	0.47	1.09	1.09	274.8	0.39	0.91
				1.98	1008.0	347.9	394.4	0.39	1.13	1.13	321.6	0.32	0.92
				2.17	1209.6	369.5	429.7	0.36	1.16	1.16	347.8	0.29	0.94
CY	0.972	0.938	240.32	1.01	245.4	182.0	182.5	0.74	1.00	1.00	160.4	0.65	0.88
				1.20	348.5	222.4	223.1	0.64	1.00	1.00	191.2	0.55	0.86
				1.50	539.9	274.4	281.1	0.52	1.02	1.02	235.1	0.44	0.86
				1.69	687.2	303.4	317.2	0.46	1.05	1.05	262.2	0.38	0.86
				2.02	981.7	346.2	376.6	0.38	1.09	1.09	306.6	0.31	0.89
				2.21	1178.1	361.3	410.2	0.35	1.14	1.14	331.5	0.28	0.92

Table A2 – Part II: Numerical ultimate loads and DSM estimates – *R135* columns analysed at *100*ºC.

σ-ε	k_y	k_e	P_{cr} (kN)	$\bar{\lambda}_D$	P_y (kN)	P_u (kN)	$P_{n.D}$ (kN)	$\frac{P_u}{P_y}$	$\frac{P_{n.D}}{P_y}$	$\frac{P_{n.D}}{P_u}$	$P^*_{n.D}$ (kN)	$\frac{P^*_{n.D}}{P_y}$	$\frac{P^*_{n.D}}{P_u}$
HR	1.000	0.900	122.37	1.20	177.5	114.9	113.6	0.65	0.64	0.99	97.4	0.55	0.85
				1.44	252.1	136.0	136.9	0.54	0.54	1.01	115.0	0.46	0.85
				1.79	390.5	147.9	170.4	0.38	0.44	1.15	140.2	0.36	0.95
				2.02	497.0	170.3	191.3	0.34	0.38	1.12	155.7	0.31	0.91
				2.41	710.0	203.4	225.7	0.29	0.32	1.11	181.3	0.26	0.89
				2.64	852.0	224.1	245.2	0.26	0.29	1.09	195.7	0.23	0.87
CF	0.939	0.860	116.93	1.19	166.7	108.0	107.5	0.65	0.65	1.00	92.3	0.55	0.85
				1.42	236.7	132.5	129.6	0.56	0.55	0.98	109.0	0.46	0.82
				1.77	366.7	146.9	161.4	0.40	0.44	1.10	132.9	0.36	0.90
				2.00	466.7	161.6	181.2	0.35	0.39	1.12	147.7	0.32	0.91
				2.39	666.7	192.4	214.0	0.29	0.32	1.11	172.0	0.26	0.89
				2.62	800.0	212.3	232.5	0.27	0.29	1.09	185.6	0.23	0.87
WJ	0.961	0.981	133.39	1.13	170.6	118.0	115.4	0.69	0.68	0.98	99.8	0.58	0.85
				1.35	242.2	139.0	139.7	0.57	0.58	1.01	118.2	0.49	0.85
				1.68	375.3	160.4	174.6	0.43	0.47	1.09	144.5	0.38	0.90
				1.89	477.6	177.6	196.3	0.37	0.41	1.11	160.7	0.34	0.90
				2.26	682.3	213.3	232.2	0.31	0.34	1.09	187.4	0.27	0.88
				2.48	818.8	234.3	252.4	0.29	0.31	1.08	202.4	0.25	0.86
RM	0.987	0.870	118.29	1.22	175.2	103.4	111.1	0.63	1.07	1.07	95.1	0.54	0.92
				1.45	248.8	124.6	133.8	0.54	1.07	1.07	112.2	0.45	0.90
				1.81	385.4	150.9	166.4	-0.43	1.10	1.10	136.7	0.35	0.91
				2.04	490.5	145.2	186.7	-0.38	1.29	1.29	151.9	0.31	1.05
				2.43	700.8	161.6	220.3	-0.31	1.36	1.36	176.8	0.25	1.09
				2.67	840.9	200.1	239.2	-0.28	1.20	1.20	190.8	0.23	0.95
CY	0.936	0.858	116.66	1.19	166.1	103.3	107.2	0.65	1.04	1.04	92.0	0.55	0.89
				1.42	235.9	123.3	129.3	0.55	1.05	1.05	108.7	0.46	0.88
				1.77	365.5	141.3	161.0	-0.44	1.14	1.14	132.5	0.36	0.94
				2.00	465.2	159.0	180.7	-0.39	1.14	1.14	147.3	0.32	0.93
				2.39	664.6	190.5	213.4	-0.32	1.12	1.12	171.5	0.26	0.90
				2.61	797.5	210.0	231.8	-0.29	1.10	1.10	185.1	0.23	0.88

Table A3 – Part I: Numerical ultimate loads and DSM estimates – *C130* columns analysed at *200*ºC.

σ-ε	k_y	k_e	P_{cr} (kN)	$\bar{\lambda}_D$	P_y (kN)	P_u (kN)	$P_{n.D}$ (kN)	$\frac{P_u}{P_y}$	$\frac{P_{n.D}}{P_y}$	$\frac{P_{n.D}}{P_u}$	$P^*_{n.D}$ (kN)	$\frac{P^*_{n.D}}{P_y}$	$\frac{P^*_{n.D}}{P_u}$
HR	1.000	0.900	230.59	1.05	252.5	201.0	182.5	0.72	0.91	0.91	159.5	0.63	0.79
				1.25	358.6	227.2	222.3	0.62	0.98	0.98	189.8	0.53	0.84
				1.55	555.5	275.1	279.4	0.50	1.02	1.02	232.9	0.42	0.85
				1.75	707.0	303.6	314.9	0.45	1.04	1.04	259.5	0.37	0.85
				2.09	1010.0	343.6	373.4	0.37	1.09	1.09	303.1	0.30	0.88
				2.29	1212.0	352.8	406.5	0.34	1.15	1.15	327.7	0.27	0.93
CF	0.939	0.860	220.34	1.04	237.1	189.3	172.6	0.73	0.91	0.91	151.0	0.64	0.80
				1.24	336.7	221.0	210.5	0.63	0.95	0.95	179.8	0.53	0.81
				1.54	521.6	264.2	264.7	0.51	1.00	1.00	220.8	0.42	0.84
				1.74	663.9	291.2	298.3	0.45	1.02	1.02	246.0	0.37	0.84
				2.07	948.4	332.9	353.9	0.37	1.06	1.06	287.5	0.30	0.86
				2.27	1138.1	350.7	385.3	0.34	1.10	1.10	310.8	0.27	0.89
WJ	0.961	0.981	251.34	0.98	242.7	185.9	184.6	0.76	0.99	0.99	162.9	0.67	0.88
				1.17	344.6	229.8	226.2	0.66	0.98	0.98	194.6	0.56	0.85
				1.46	533.8	283.2	285.7	0.54	1.01	1.01	239.6	0.45	0.85
				1.64	679.4	313.0	322.6	0.47	1.03	1.03	267.4	0.39	0.85
				1.97	970.6	358.5	383.5	0.40	1.07	1.07	312.9	0.32	0.87
				2.15	1164.7	375.5	417.9	0.36	1.11	1.11	338.5	0.29	0.90
RM	0.987	0.870	222.90	1.06	249.2	173.3	178.6	0.72	1.03	1.03	155.8	0.63	0.90
				1.26	353.9	209.3	217.4	0.61	1.04	1.04	185.3	0.52	0.89
				1.57	548.3	269.9	273.0	0.50	1.01	1.01	227.2	0.41	0.84
				1.77	697.8	275.8	307.5	0.44	1.11	1.11	253.1	0.36	0.92
				2.11	996.9	277.5	364.5	0.37	1.31	1.31	295.7	0.30	1.07
				2.32	1196.2	330.3	396.7	0.33	1.20	1.20	319.6	0.27	0.97
CY	0.936	0.858	219.83	1.04	236.3	168.1	172.1	0.73	1.02	1.02	150.6	0.64	0.90
				1.24	335.6	206.2	209.9	0.63	1.02	1.02	179.3	0.53	0.87
				1.54	519.9	253.7	263.9	0.51	1.04	1.04	220.1	0.42	0.87
				1.74	661.8	281.4	297.5	0.45	1.06	1.06	245.4	0.37	0.87
				2.07	945.4	322.8	352.9	0.37	1.09	1.09	286.7	0.30	0.89
				2.27	1134.4	335.5	384.2	0.34	1.15	1.15	310.0	0.27	0.92

Table A3 – Part II: Numerical ultimate loads and DSM estimates – *R135* columns analysed at *200*ºC.

σ-ε	k_y	k_e	P_{cr} (kN)	$\bar{\lambda}_D$	P_y (kN)	P_u (kN)	$P_{n.D}$ (kN)	$\frac{P_u}{P_y}$	$\frac{P_{n.D}}{P_y}$	$\frac{P_{n.D}}{P_u}$	$P^*_{n.D}$ (kN)	$\frac{P^*_{n.D}}{P_y}$	$\frac{P^*_{n.D}}{P_u}$
HR	1.000	0.800	108.78	1.28	177.5	102.9	107.7	0.58	0.61	1.05	91.6	0.52	0.89
				1.52	252.1	121.9	129.2	0.48	0.51	1.06	107.9	0.43	0.89
				1.89	390.5	132.8	160.3	0.34	0.41	1.21	131.2	0.34	0.99
				2.14	497.0	134.8	179.7	0.27	0.36	1.33	145.6	0.29	1.08
				2.55	710.0	161.6	211.7	0.23	0.30	1.31	169.3	0.24	1.05
				2.80	852.0	212.4	229.8	0.25	0.27	1.08	182.7	0.21	0.86
CF	0.860	0.720	97.90	1.25	152.7	88.7	94.5	0.58	0.62	1.07	80.7	0.53	0.91
				1.49	216.8	110.0	113.7	0.51	0.52	1.03	95.1	0.44	0.86
				1.85	335.8	127.5	141.2	0.38	0.42	1.11	115.8	0.34	0.91
				2.09	427.4	137.7	158.3	0.32	0.37	1.15	128.5	0.30	0.93
				2.50	610.6	164.4	186.6	0.27	0.31	1.14	149.5	0.24	0.91
				2.74	732.7	181.2	202.6	0.25	0.28	1.12	161.3	0.22	0.89
WJ	0.926	0.928	126.18	1.14	164.4	114.3	110.3	0.70	0.67	0.97	95.2	0.58	0.83
				1.36	233.4	134.1	133.5	0.57	0.57	1.00	112.8	0.48	0.84
				1.69	361.6	152.7	166.7	0.42	0.46	1.09	137.8	0.38	0.90
				1.91	460.2	169.9	187.4	0.37	0.41	1.10	153.2	0.33	0.90
				2.28	657.5	209.5	221.5	0.32	0.34	1.06	178.6	0.27	0.85
				2.50	789.0	223.9	240.8	0.28	0.31	1.08	192.9	0.24	0.86
RM	0.899	0.740	100.62	1.26	159.6	91.1	98.1	0.61	1.08	1.08	83.6	0.52	0.92
				1.50	226.6	108.5	117.8	0.52	1.09	1.09	98.5	0.43	0.91
				1.87	351.1	131.3	146.3	0.42	1.11	1.11	119.9	0.34	0.91
				2.11	446.8	123.3	164.0	0.37	1.33	1.33	133.1	0.30	1.08
				2.52	638.3	125.7	193.3	0.30	1.54	1.54	154.8	0.24	1.23
				2.76	765.9	176.2	209.9	0.27	1.19	1.19	167.0	0.22	0.95
CY	0.900	0.778	105.78	1.23	159.8	95.4	100.4	0.63	1.05	1.05	85.8	0.54	0.90
				1.46	226.8	113.0	120.8	0.53	1.07	1.07	101.3	0.45	0.90
				1.82	351.5	130.8	150.2	0.43	1.15	1.15	123.3	0.35	0.94
				2.06	447.3	147.8	168.5	0.38	1.14	1.14	137.0	0.31	0.93
				2.46	639.0	177.0	198.7	0.31	1.12	1.12	159.4	0.25	0.90
				2.69	766.8	195.6	215.8	0.28	1.10	1.10	172.0	0.22	0.88

Table A4 – Part I: Numerical ultimate loads and DSM estimates – *C130* columns analysed at *300*ºC.

σ-ε	k_y	k_e	P_{cr} (kN)	$\bar{\lambda}_D$	P_y (kN)	P_u (kN)	$P_{n.D}$ (kN)	$\frac{P_u}{P_y}$	$\frac{P_{n.D}}{P_y}$	$\frac{P_{n.D}}{P_u}$	$P^*_{n.D}$ (kN)	$\frac{P^*_{n.D}}{P_y}$	$\frac{P^*_{n.D}}{P_u}$
HR	1.000	0.800	204.97	1.11	252.5	177.7	173.7	0.69	0.98	0.98	150.5	0.60	0.85
				1.32	358.6	204.1	210.5	0.59	1.03	1.03	178.4	0.50	0.87
				1.65	555.5	246.7	263.4	0.47	1.07	1.07	218.3	0.39	0.88
				1.86	707.0	271.8	296.3	0.42	1.09	1.09	242.9	0.34	0.89
				2.22	1010.0	307.8	350.7	0.35	1.14	1.14	283.4	0.28	0.92
				2.43	1212.0	314.5	381.4	0.31	1.21	1.21	306.1	0.25	0.97
CF	0.860	0.720	184.47	1.08	217.2	148.5	152.3	0.70	1.03	1.03	132.4	0.61	0.89
				1.29	308.4	187.5	184.9	0.60	0.99	0.99	157.2	0.51	0.84
				1.61	477.7	222.7	231.8	0.49	1.04	1.04	192.5	0.40	0.86
				1.82	608.0	246.5	260.9	0.43	1.06	1.06	214.3	0.35	0.87
				2.17	868.6	285.6	309.0	0.36	1.08	1.08	250.1	0.29	0.88
				2.38	1042.3	302.7	336.2	0.32	1.11	1.11	270.3	0.26	0.89
WJ	0.926	0.928	237.76	0.99	233.8	182.4	176.5	0.76	0.97	0.97	155.6	0.67	0.85
				1.18	332.0	222.4	216.1	0.65	0.97	0.97	185.7	0.56	0.84
				1.47	514.4	271.7	272.8	0.53	1.00	1.00	228.6	0.44	0.84
				1.66	654.7	300.3	308.0	0.47	1.03	1.03	255.0	0.39	0.85
				1.98	935.3	342.0	366.0	0.39	1.07	1.07	298.4	0.32	0.87
				2.17	1122.3	357.7	398.7	0.36	1.11	1.11	322.8	0.29	0.90
RM	0.899	0.740	189.60	1.09	227.0	151.5	158.0	0.70	1.04	1.04	137.2	0.60	0.91
				1.30	322.3	179.9	191.8	0.60	1.07	1.07	162.8	0.51	0.91
				1.62	499.4	234.4	240.2	0.48	1.03	1.03	199.4	0.40	0.85
				1.83	635.6	239.3	270.4	0.43	1.13	1.13	221.9	0.35	0.93
				2.19	908.0	271.4	320.1	0.35	1.18	1.18	259.0	0.29	0.95
				2.40	1089.6	283.4	348.2	0.32	1.23	1.23	279.8	0.26	0.99
CY	0.900	0.778	199.33	1.07	227.3	154.4	161.5	0.71	1.05	1.05	140.7	0.62	0.91
				1.27	322.7	189.8	196.4	0.61	1.04	1.04	167.3	0.52	0.88
				1.58	500.0	234.1	246.5	0.49	1.05	1.05	205.0	0.41	0.88
				1.79	636.3	259.4	277.6	0.44	1.07	1.07	228.3	0.36	0.88
				2.14	909.0	293.0	328.9	0.36	1.12	1.12	266.6	0.29	0.91
				2.34	1090.8	301.1	357.9	0.33	1.19	1.19	288.1	0.26	0.96

Table A4 – Part II: Numerical ultimate loads and DSM estimates – *R135* columns analysed at *300*ºC.

σ-ε	k_y	k_e	P_{cr} (kN)	$\bar{\lambda}_D$	P_y (kN)	P_u (kN)	$P_{n.D}$ (kN)	$\frac{P_u}{P_y}$	$\frac{P_{n.D}}{P_y}$	$\frac{P_{n.D}}{P_u}$	$P^*_{n.D}$ (kN)	$\frac{P^*_{n.D}}{P_y}$	$\frac{P^*_{n.D}}{P_u}$
HR	1.000	0.700	95.18	1.37	177.5	90.5	101.1	0.51	0.57	1.12	81.2	0.46	0.90
				1.63	252.1	106.8	120.9	0.42	0.48	1.13	94.3	0.37	0.88
				2.03	390.5	116.8	149.5	0.30	0.38	1.28	112.4	0.29	0.96
				2.29	497.0	127.7	167.3	0.26	0.34	1.31	123.5	0.25	0.97
				2.73	710.0	142.0	196.7	0.20	0.28	1.39	141.4	0.20	1.00
				2.99	852.0	189.4	213.4	0.22	0.25	1.13	151.3	0.18	0.80
CF	0.729	0.580	78.86	1.28	129.4	68.6	78.3	0.53	0.60	1.14	63.6	0.49	0.93
				1.53	183.7	85.7	94.0	0.47	0.51	1.10	74.0	0.40	0.86
				1.90	284.7	107.6	116.5	0.38	0.41	1.08	88.5	0.31	0.82
				2.14	362.3	114.3	130.6	0.32	0.36	1.14	97.4	0.27	0.85
				2.56	517.6	134.0	153.9	0.26	0.30	1.15	111.6	0.22	0.83
				2.81	621.1	148.3	167.0	0.24	0.27	1.13	119.6	0.19	0.81
WJ	0.743	0.820	111.50	1.09	131.9	88.2	92.3	0.67	0.70	1.05	77.4	0.59	0.88
				1.30	187.3	110.0	112.1	0.59	0.60	1.02	90.9	0.49	0.83
				1.61	290.1	130.2	140.4	0.45	0.48	1.08	109.6	0.38	0.84
				1.82	369.3	141.6	158.1	0.38	0.43	1.12	120.9	0.33	0.85
				2.18	527.5	170.9	187.2	0.32	0.35	1.10	139.2	0.26	0.81
				2.38	633.0	193.3	203.6	0.31	0.32	1.05	149.4	0.24	0.77
RM	0.717	0.610	82.94	1.24	127.3	73.3	79.4	0.62	1.08	1.08	64.9	0.51	0.89
				1.48	180.7	87.8	95.5	0.53	1.09	1.09	75.7	0.42	0.86
				1.84	280.0	106.5	118.7	0.42	1.11	1.11	90.7	0.32	0.85
				2.07	356.3	101.6	133.1	0.37	1.31	1.31	99.8	0.28	0.98
				2.48	509.1	104.4	157.0	0.31	1.50	1.50	114.5	0.22	1.10
				2.71	610.9	141.7	170.4	0.28	1.20	1.20	122.6	0.20	0.87
CY	0.692	0.698	94.91	1.14	122.8	75.9	82.7	0.67	1.09	1.09	68.7	0.56	0.91
				1.36	174.4	92.7	100.1	0.57	1.08	1.08	80.5	0.46	0.87
				1.69	270.2	109.9	125.0	0.46	1.14	1.14	96.8	0.36	0.88
				1.90	343.9	121.2	140.5	0.41	1.16	1.16	106.7	0.31	0.88
				2.28	491.3	145.9	166.1	0.34	1.14	1.14	122.7	0.25	0.84
				2.49	589.6	160.7	180.6	0.31	1.12	1.12	131.6	0.22	0.82

Table A5 – Part I: Numerical ultimate loads and DSM estimates – *C130* columns analysed at *400*ºC.

σ-ε	k_y	k_e	P_{cr} (kN)	$\bar{\lambda}_D$	P_y (kN)	P_u (kN)	$P_{n.D}$ (kN)	$\frac{P_u}{P_y}$	$\frac{P_{n.D}}{P_y}$	$\frac{P_{n.D}}{P_u}$	$P^*_{n.D}$ (kN)	$\frac{P^*_{n.D}}{P_y}$	$\frac{P^*_{n.D}}{P_u}$
HR	1.000	0.700	179.35	1.19	252.5	151.7	163.8	0.65	1.08	1.08	135.0	0.53	0.89
				1.41	358.6	178.5	197.6	0.55	1.11	1.11	157.8	0.44	0.88
				1.76	555.5	217.0	246.1	0.44	1.13	1.13	189.4	0.34	0.87
				1.99	707.0	241.7	276.4	0.39	1.14	1.14	208.5	0.29	0.86
				2.37	1010.0	270.3	326.3	0.32	1.21	1.21	239.5	0.24	0.89
				2.60	1212.0	276.3	354.5	0.29	1.28	1.28	256.7	0.21	0.93
CF	0.729	0.580	148.60	1.11	184.1	104.7	126.3	0.69	1.21	1.21	105.4	0.57	1.01
				1.33	261.4	142.8	153.1	0.59	1.07	1.07	123.6	0.47	0.87
				1.65	405.0	179.1	191.5	0.47	1.07	1.07	148.9	0.37	0.83
				1.86	515.4	199.1	215.4	0.42	1.08	1.08	164.2	0.32	0.82
				2.23	736.3	233.8	254.9	0.35	1.09	1.09	188.9	0.26	0.81
				2.44	883.5	251.9	277.2	0.31	1.10	1.10	202.6	0.23	0.80
WJ	0.743	0.820	210.09	0.94	187.6	140.6	147.1	0.78	1.05	1.05	127.0	0.68	0.90
				1.13	266.4	178.3	180.9	0.68	1.01	1.01	150.7	0.57	0.85
				1.40	412.7	224.2	229.4	0.56	1.02	1.02	183.4	0.44	0.82
				1.58	525.3	249.2	259.4	0.49	1.04	1.04	203.1	0.39	0.82
				1.89	750.4	289.6	308.9	0.41	1.07	1.07	234.9	0.31	0.81
				2.07	900.5	306.1	336.8	0.37	1.10	1.10	252.5	0.28	0.82
RM	0.717	0.610	156.29	1.08	181.0	120.9	127.8	0.71	1.06	1.06	107.4	0.59	0.89
				1.28	257.1	145.6	155.3	0.60	1.07	1.07	126.2	0.49	0.87
				1.60	398.3	189.1	194.8	0.49	1.03	1.03	152.3	0.38	0.81
				1.80	506.9	193.9	219.3	0.43	1.13	1.13	168.1	0.33	0.87
				2.15	724.2	220.8	259.8	0.36	1.18	1.18	193.6	0.27	0.88
				2.36	869.0	231.5	282.7	0.33	1.22	1.22	207.7	0.24	0.90
CY	0.692	0.698	178.83	0.99	174.7	121.3	132.3	0.76	1.09	1.09	113.1	0.65	0.93
				1.18	248.1	152.2	162.0	0.65	1.06	1.06	133.8	0.54	0.88
				1.47	384.4	193.2	204.5	0.53	1.06	1.06	162.3	0.42	0.84
				1.65	489.2	215.1	230.9	0.47	1.07	1.07	179.5	0.37	0.83
				1.98	698.9	251.7	274.5	0.39	1.09	1.09	207.2	0.30	0.82
				2.17	838.7	261.7	299.0	0.36	1.14	1.14	222.6	0.27	0.85

Table A5 – Part II: Numerical ultimate loads and DSM estimates – *R135* columns analysed at *400*ºC.

σ-ε	k_y	k_e	P_{cr} (kN)	$\bar{\lambda}_D$	P_y (kN)	P_u (kN)	$P_{n.D}$ (kN)	$\frac{P_u}{P_y}$	$\frac{P_{n.D}}{P_y}$	$\frac{P_{n.D}}{P_u}$	$P^*_{n.D}$ (kN)	$\frac{P^*_{n.D}}{P_y}$	$\frac{P^*_{n.D}}{P_u}$
HR	0.780	0.600	81.58	1.30	138.5	74.5	82.5	0.54	0.60	1.11	66.8	0.48	0.90
				1.55	196.6	89.4	98.9	0.45	0.50	1.11	77.7	0.40	0.87
				1.93	304.6	102.2	122.5	0.34	0.40	1.20	92.8	0.30	0.91
				2.18	387.7	101.5	137.2	0.26	0.35	1.35	102.1	0.26	1.01
				2.61	553.8	120.5	161.6	0.22	0.29	1.34	117.0	0.21	0.97
				2.85	664.6	155.4	175.4	0.23	0.26	1.13	125.3	0.19	0.81
CF	0.550	0.440	59.83	1.28	97.6	58.7	59.2	0.60	0.61	1.01	48.2	0.49	0.82
				1.52	138.6	73.0	71.1	0.53	0.51	0.97	56.0	0.40	0.77
				1.89	214.8	92.2	88.2	0.43	0.41	0.96	67.0	0.31	0.73
				2.14	273.4	97.1	98.8	0.36	0.36	1.02	73.7	0.27	0.76
				2.55	390.5	113.2	116.4	0.29	0.30	1.03	84.5	0.22	0.75
				2.80	468.6	124.8	126.4	0.27	0.27	1.01	90.5	0.19	0.73
WJ	0.482	0.587	79.81	1.04	85.6	58.6	62.4	0.69	0.73	1.06	52.9	0.62	0.90
				1.23	121.5	74.2	76.1	0.61	0.63	1.03	62.3	0.51	0.84
				1.54	188.2	89.9	95.7	0.48	0.51	1.06	75.3	0.40	0.84
				1.73	239.6	97.0	107.9	0.40	0.45	1.11	83.2	0.35	0.86
				2.07	342.2	115.9	128.0	0.34	0.37	1.10	95.9	0.28	0.83
				2.27	410.7	127.7	139.3	0.31	0.34	1.09	103.0	0.25	0.81
RM	0.462	0.480	65.27	1.12	82.0	51.0	55.9	0.68	1.10	1.10	46.6	0.57	0.91
				1.34	116.4	63.2	67.7	0.58	1.07	1.07	54.6	0.47	0.86
				1.66	180.4	78.2	84.7	0.47	1.08	1.08	65.8	0.36	0.84
				1.88	229.6	78.5	95.3	0.41	1.21	1.21	72.5	0.32	0.92
				2.24	328.0	94.8	112.7	0.34	1.19	1.19	83.4	0.25	0.88
				2.46	393.6	104.0	122.5	0.31	1.18	1.18	89.5	0.23	0.86
CY	0.159	0.479	65.13	0.66	28.2	21.4	27.4	0.97	1.28	1.28	26.0	0.92	1.21
				0.78	40.1	28.5	35.7	0.89	1.25	1.25	32.2	0.80	1.13
				0.98	62.1	40.7	47.5	0.76	1.17	1.17	40.7	0.66	1.00
				1.10	79.0	48.6	54.7	0.69	1.13	1.13	45.8	0.58	0.94
				1.32	112.9	60.9	66.6	0.59	1.09	1.09	53.8	0.48	0.88
				1.44	135.5	66.4	73.2	0.54	1.10	1.10	58.3	0.43	0.88

Table A6 – Part I: Numerical ultimate loads and DSM estimates – *C130* columns analysed at *500*ºC.

σ-ε	k_y	k_e	P_{cr} (kN)	$\bar{\lambda}_D$	P_y (kN)	P_u (kN)	$P_{n.D}$ (kN)	$\frac{P_u}{P_y}$	$\frac{P_{n.D}}{P_y}$	$\frac{P_{n.D}}{P_u}$	$P^*_{n.D}$ (kN)	$\frac{P^*_{n.D}}{P_y}$	$\frac{P^*_{n.D}}{P_u}$
HR	0.780	0.600	153.73	1.13	197.0	125.2	133.2	0.68	1.06	1.06	110.8	0.56	0.89
				1.35	279.7	147.4	161.2	0.58	1.09	1.09	129.8	0.46	0.88
				1.68	433.3	180.1	201.4	0.46	1.12	1.12	156.2	0.36	0.87
				1.89	551.5	201.1	226.5	0.41	1.13	1.13	172.2	0.31	0.86
				2.26	787.8	226.3	267.8	0.34	1.18	1.18	198.0	0.25	0.87
				2.48	945.4	234.5	291.2	0.31	1.24	1.24	212.3	0.22	0.91
CF	0.550	0.440	112.73	1.11	138.9	89.7	95.5	0.69	1.07	1.07	79.8	0.57	0.89
				1.32	197.2	122.2	115.8	0.59	0.95	0.95	93.6	0.47	0.77
				1.65	305.5	152.0	144.9	0.47	0.95	0.95	112.7	0.37	0.74
				1.86	388.9	169.6	163.0	0.42	0.96	0.96	124.3	0.32	0.73
				2.22	555.5	198.5	192.9	0.35	0.97	0.97	143.0	0.26	0.72
				2.43	666.6	214.1	209.7	0.31	0.98	0.98	153.4	0.23	0.72
WJ	0.482	0.587	150.40	0.90	121.7	92.1	99.0	0.81	1.07	1.07	86.4	0.71	0.94
				1.07	172.8	119.2	122.4	0.71	1.03	1.03	103.0	0.60	0.86
				1.33	267.8	152.0	155.9	0.58	1.03	1.03	125.8	0.47	0.83
				1.51	340.8	170.0	176.7	0.52	1.04	1.04	139.5	0.41	0.82
				1.80	486.8	200.2	210.9	0.43	1.05	1.05	161.6	0.33	0.81
				1.97	584.2	214.2	230.1	0.39	1.07	1.07	173.9	0.30	0.81
RM	0.462	0.480	122.98	0.97	116.7	82.2	89.3	0.77	1.09	1.09	76.7	0.66	0.93
				1.16	165.7	104.5	109.6	0.66	1.05	1.05	90.7	0.55	0.87
				1.44	256.6	139.1	138.5	0.54	1.00	1.00	110.2	0.43	0.79
				1.63	326.6	141.2	156.5	0.48	1.11	1.11	121.9	0.37	0.86
				1.95	466.6	163.1	186.1	0.40	1.14	1.14	140.8	0.30	0.86
				2.13	559.9	174.2	202.8	0.36	1.16	1.16	151.3	0.27	0.87
CY	0.159	0.479	122.72	0.57	40.1	32.2	40.1	1.00	1.24	1.24	40.0	1.00	1.24
				0.68	57.0	44.3	54.5	0.96	1.23	1.23	51.2	0.90	1.16
				0.85	88.3	63.7	74.8	0.85	1.17	1.17	66.2	0.75	1.04
				0.96	112.4	77.2	87.3	0.78	1.13	1.13	75.2	0.67	0.97
				1.14	160.6	98.2	107.6	0.67	1.10	1.10	89.3	0.56	0.91
				1.25	192.7	110.0	119.0	0.62	1.08	1.08	97.1	0.50	0.88

Table A6 – Part II: Numerical ultimate loads and DSM estimates – *R135* columns analysed at *500*ºC.

σ-ε	k_y	k_e	P_{cr} (kN)	$\bar{\lambda}_D$	P_y (kN)	P_u (kN)	$P_{n.D}$ (kN)	$\frac{P_u}{P_y}$	$\frac{P_{n.D}}{P_y}$	$\frac{P_{n.D}}{P_u}$	$P^*_{n.D}$ (kN)	$\frac{P^*_{n.D}}{P_y}$	$\frac{P^*_{n.D}}{P_u}$
HR	0.470	0.310	42.15	1.41	83.4	40.8	46.2	0.49	0.55	1.13	36.9	0.44	0.90
				1.68	118.5	48.0	55.2	0.41	0.47	1.15	42.8	0.36	0.89
				2.09	183.5	56.0	68.1	0.31	0.37	1.22	51.0	0.28	0.91
				2.35	233.6	58.2	76.1	0.25	0.33	1.31	55.9	0.24	0.96
				2.81	333.7	78.3	89.5	0.23	0.27	1.14	64.0	0.19	0.82
				3.56	533.9	86.4	110.0	0.16	0.21	1.27	76.1	0.14	0.88
CF	0.350	0.281	38.21	1.28	62.1	30.1	37.7	0.48	0.61	1.25	30.7	0.49	1.02
				1.52	88.2	37.5	45.3	0.42	0.51	1.21	35.7	0.41	0.95
				1.89	136.7	47.0	56.2	0.34	0.41	1.20	42.7	0.31	0.91
				2.13	174.0	50.3	63.0	0.29	0.36	1.25	47.0	0.27	0.93
				2.55	248.5	59.7	74.2	0.24	0.30	1.24	53.9	0.22	0.90
				2.79	298.2	66.2	80.6	0.22	0.27	1.22	57.7	0.19	0.87
WJ	0.057	0.281	38.21	0.51	10.1	9.1	10.1	0.90	1.00	1.12	10.1	1.00	1.12
				0.61	14.4	12.7	14.2	0.88	0.99	1.12	13.8	0.96	1.09
				0.76	22.3	18.9	20.1	0.85	0.90	1.06	18.3	0.82	0.97
				0.86	28.3	23.2	23.8	0.82	0.84	1.02	21.0	0.74	0.90
				1.03	40.5	29.5	29.7	0.73	0.73	1.00	25.2	0.62	0.85
				1.13	48.6	33.5	33.0	0.69	0.68	0.98	27.4	0.57	0.82
RM	0.192	0.350	47.59	0.85	34.1	25.2	28.9	0.85	1.15	1.15	25.6	0.75	1.02
				1.01	48.4	32.6	36.1	0.74	1.11	1.11	30.7	0.63	0.94
				1.26	75.0	47.6	46.2	0.62	0.97	0.97	37.7	0.50	0.79
				1.42	95.4	48.6	52.5	0.55	1.08	1.08	41.9	0.44	0.86
				1.69	136.3	55.2	62.9	0.46	1.14	1.14	48.7	0.36	0.88
				1.85	163.6	57.5	68.7	0.42	1.19	1.19	52.4	0.32	0.91
CY	0.091	0.197	26.79	0.78	16.2	10.0	14.5	0.90	1.45	1.45	13.1	0.81	1.31
				0.93	22.9	14.7	18.3	0.80	1.24	1.24	15.9	0.69	1.08
				1.15	35.5	20.7	23.7	0.67	1.14	1.14	19.6	0.55	0.95
				1.30	45.2	24.0	27.0	0.60	1.13	1.13	21.9	0.48	0.91
				1.55	64.6	28.4	32.5	0.50	1.14	1.14	25.5	0.39	0.90
				1.70	77.5	30.6	35.6	0.46	1.16	1.16	27.5	0.35	0.90

Table A7 – Part I: Numerical ultimate loads and DSM estimates – *C130* columns analysed at *600*ºC.

σ-ε	k_y	k_E	P_{cr} (kN)	$\bar{\lambda}_D$	P_y (kN)	P_u (kN)	$P_{n.D}$ (kN)	$\frac{P_u}{P_y}$	$\frac{P_{n.D}}{P_y}$	$\frac{P_{n.D}}{P_u}$	$P^*_{n.D}$ (kN)	$\frac{P^*_{n.D}}{P_y}$	$\frac{P^*_{n.D}}{P_u}$
HR	0.470	0.310	79.43	1.22	118.7	68.1	74.9	0.63	1.10	1.10	61.4	0.52	0.90
				1.46	168.5	81.7	90.2	0.54	1.10	1.10	71.7	0.43	0.88
				1.81	261.1	97.8	112.2	0.43	1.15	1.15	85.9	0.33	0.88
				2.05	332.3	108.5	125.9	0.38	1.16	1.16	94.5	0.28	0.87
				2.44	474.7	119.8	148.5	0.31	1.24	1.24	108.5	0.23	0.91
				2.68	569.6	122.2	161.3	0.28	1.32	1.32	116.3	0.20	0.95
CF	0.350	0.281	72.00	1.11	88.4	45.1	60.9	0.69	1.35	1.35	50.9	0.58	1.13
				1.32	125.5	61.7	73.8	0.59	1.20	1.20	59.7	0.48	0.97
				1.64	194.4	78.4	92.4	0.48	1.18	1.18	71.9	0.37	0.92
				1.85	247.5	87.8	103.9	0.42	1.18	1.18	79.3	0.32	0.90
				2.22	353.5	102.9	123.0	0.35	1.19	1.19	91.2	0.26	0.89
				2.43	424.2	110.8	133.7	0.32	1.21	1.21	97.8	0.23	0.88
WJ	0.057	0.281	72.00	0.45	14.4	13.1	14.4	1.00	1.10	1.10	14.4	1.00	1.10
				0.53	20.4	18.3	20.4	1.00	1.11	1.11	20.4	1.00	1.11
				0.66	31.7	27.8	30.6	0.97	1.10	1.10	29.0	0.91	1.04
				0.75	40.3	34.9	36.9	0.91	1.06	1.06	33.7	0.84	0.97
				0.89	57.6	47.8	47.0	0.82	0.98	0.98	41.1	0.71	0.86
				0.98	69.1	55.4	52.7	0.76	0.95	0.95	45.1	0.65	0.81
RM	0.192	0.350	89.67	0.74	48.5	37.1	44.8	0.92	1.21	1.21	41.1	0.85	1.11
				0.88	68.8	50.6	57.0	0.83	1.13	1.13	50.1	0.73	0.99
				1.09	106.7	78.9	74.5	0.70	0.94	0.94	62.4	0.59	0.79
				1.23	135.7	81.1	85.2	0.63	1.05	1.05	69.8	0.51	0.86
				1.47	193.9	94.7	102.9	0.53	1.09	1.09	81.6	0.42	0.86
				1.61	232.7	102.1	112.8	0.48	1.10	1.10	88.1	0.38	0.86
CY	0.091	0.197	50.47	0.67	23.0	17.0	22.1	0.96	1.30	1.30	20.8	0.90	1.22
				0.80	32.6	23.6	28.6	0.88	1.22	1.22	25.7	0.79	1.09
				1.00	50.6	32.8	37.9	0.75	1.16	1.16	32.3	0.64	0.99
				1.13	64.3	38.7	43.6	0.68	1.13	1.13	36.3	0.56	0.94
				1.35	91.9	48.0	53.0	0.58	1.10	1.10	42.6	0.46	0.89
				1.48	110.3	52.7	58.2	0.53	1.10	1.10	46.1	0.42	0.88

Table A7 – Part II: Numerical ultimate loads and DSM estimates – *R135* columns analysed at *600*ºC.